AGU PUBLICATIONS

JGR

Journal of Geophysical Research: Biogeosciences

RESEARCH ARTICLE
10.1002/2015JG003279

Key Points:
- TC timing and trajectory determine the magnitude of impact on GPP across and within years
- In wet years, TCs impact plant activity in 40–50% of the SE U.S. and increase GPP by 3–5 Mg C/m^2/yr
- In wet years, the increase in GPP associated with TCs is 9% of warm season carbon assimilated in the SE U.S.

Supporting Information:
- Supporting Information S1
- Figure S1
- Figure S2
- Figure S3
- Figure S4
- Figure S5
- Movie S1

Correspondence to:
A. P. Barros,
barros@duke.edu

Citation:
Lowman, L. E. L., and A. P. Barros (2016), Interplay of drought and tropical cyclone activity in SE U.S. gross primary productivity, *J. Geophys. Res. Biogeosci.*, *121*, 1540–1567, doi:10.1002/2015JG003279.

Received 16 NOV 2015
Accepted 12 APR 2016
Accepted article online 19 APR 2016
Published online 18 JUN 2016
Corrected 15 SEP 2016

This article was corrected on 15 SEP 2016. See the end of the full text for details.

Interplay of drought and tropical cyclone activity in SE U.S. gross primary productivity

Lauren E. L. Lowman[1] **and Ana P. Barros**[1]

[1]Department of Civil and Environmental Engineering, Duke University, Durham, North Carolina, USA

Abstract Tropical cyclones (TCs), often associated with massive flooding and landslides in the Southeast U.S. (SE U.S.), provide a significant input of freshwater to the hydrologic system, and their timing and trajectory significantly impact drought severity and persistence. This manuscript investigates the sensitivity of gross primary productivity (GPP) in the SE U.S. to TC activity using the 1-D column implementation of the Duke Coupled Hydrology Model with Vegetation (DCHM-V) including coupled water and energy cycles and a biochemical representation of photosynthesis. Decadal-scale simulations of water, energy, and carbon fluxes were conducted at high temporal (30 min) and spatial (4 km) resolution over the period 2002–2012. At local scales, model results without calibration compare well against AmeriFlux tower data. At regional scales, differences between the DCHM-V estimates and the Moderate Resolution Imaging Spectroradiometer GPP product reflect the spatial organization of soil hydraulic properties and soil moisture dynamics by physiographic region, highlighting the links between the water and carbon cycles. To isolate the contribution of TC precipitation to SE U.S. productivity, control forcing simulations are contrasted with simulations where periods of TC activity in the atmospheric forcing data were replaced with climatology. During wet years, TC activity impacts productivity in 40–50% of the SE U.S. domain and explains a regional GPP increase of 3–5 Mg C/m^2 that is 9% of the warm season total. In dry years, 23–34% of the domain exhibits a smaller positive response that corresponds to 4–8% of the seasonal carbon uptake, depending on TC timing and trajectory.

1. Introduction

Tropical cyclones (TCs) are low-pressure systems of tropical or subtropical origin with organized convection that produce heavy rainfall over extended periods of time [*Henderson-Sellers et al.*, 1998]. TC rainfall leads to floods and landslides that have devastating impacts on human life, infrastructure, and natural vegetation. Beyond this association with natural hazards, TC precipitation can represent a significant fraction of annual precipitation at the watershed scale in the Southeast United States (SE U.S.) and plays an important role in drought remission [*Brun and Barros*, 2014]. The literature is rich in reports examining changes in TC activity in response to increases in greenhouse gases in the atmosphere [e.g., *Emanuel*, 1987; *Lighthill et al.*, 1994; *Knutson and Tuleya*, 2004; *Held and Zhao*, 2011; *Kim et al.*, 2014, among others]. However, little attention has been paid to the role TCs play in carbon budgets at local, regional, or global scales. This is of particular concern to the SE U.S. (defined here as the continental U.S. below 37.75°N and east of 92.5°W) where the frequency and intensity of TC activity is expected to increase in the future [*Elsner et al.*, 2008; *Kossin et al.*, 2014], along with higher susceptibility to drought due to higher air temperature and longer storm interarrival times [*Melillo et al.*, 2014]. In this manuscript, we investigate how TCs impact and modify vegetation activity (i.e., photosynthesis and carbon assimilation) in the SE U.S. for current climate conditions by modeling water and energy fluxes between 2002 and 2012 with and without TC weather in the forcing data sets.

Thunderstorms associated with TC convection provide an important service to coastal and inland areas by delivering freshwater resources, with the heaviest rainfall from TCs occurring near and up to 500 km away from the eye track of the storm [*Barlow*, 2011; *Villarini et al.*, 2011; *Galarneau et al.*, 2010; *Hart and Evans*, 2001]. Approximately 30–40% of total monthly rainfall during the warm season in the eastern U.S. and 15% of total hurricane season rainfall in parts of the Carolinas are provided by TCs [*Cry*, 1967; *Knight and Davis*, 2007; *Nogueira and Keim*, 2010]. In the eastern Carolinas, the majority of the heaviest precipitation events are associated with TCs [*Konrad and Perry*, 2010]. *Brun and Barros* [2014] characterized the interannual variability in TC precipitation at the basin scale within 500 km of TC tracks for about 4000 watersheds and estimated TC contribution to annual rainfall totals as low as 5% in dry years and as high as 70% in wet years with a large number of landfalling TCs.

The role of TCs in drought amelioration in the SE U.S. has been well documented. *Maxwell et al.* [2012] estimated that between 1950 and 2008, 20% of drought periods were alleviated by TC precipitation over a large portion of the SE U.S. In simulations with and without TC-related precipitation over 1980–2007 using the Variable Infiltration Capacity (VIC) land surface hydrologic model, *Kam et al.* [2012] showed that soil moisture droughts are shorter in duration and impact smaller areas when there is TC activity. *Brun and Barros* [2013] tracked the temporal evolution of remote-sensing vegetation indices (e.g., Moderate Resolution Imaging Spectroradiometer (MODIS) enhanced vegetation index) before and after TC passage and found that TC precipitation effectively erased the signature of water stress shortly after storm passage in areas away from the coast and along the floodplains of large rivers where persistent vegetation disturbances due to flooding or high winds occur. Indeed, individual storms can completely redress preexisting precipitation deficits in individual basins in the SE U.S. [*Brun and Barros*, 2014].

Previous studies considered how TCs impact the carbon cycle by altering carbon storage in forests, particularly focusing on hurricane wind hazards and tree biomass losses due to mortality. *McNulty* [2002] showed that a single hurricane can reduce short-term forest carbon storage by converting 10% of total annual carbon uptake into downed biomass; however, this study only considered four hurricanes that made landfall along the eastern U.S. before 1996 and estimated the amount of carbon transferred from living to dead pools from aerial surveys. *Chambers et al.* [2007] estimated tree morality and damage caused by Hurricane Katrina at landfall in the Pearl River basin to represent 50–140% of the net annual U.S. forest tree carbon sink based on Landsat-MODIS scaling of tree mortality and damage. Using an inventory of field measurements, satellite imagery, empirical models, and historical TC data from 1951 to 2000, *Zeng et al.* [2009] found that the CO_2 released by downed trees offset the U.S. carbon sink in forest trees by 9–18%. In Australia, the impact of TC Monica, an extreme cyclone event, on tropical savannas was a reduction in gross primary productivity of about 0.5 Tg C over a 4 year period due to tree mortality and fires, estimated by comparing MODIS GPP data before and after the storm [*Hutley et al.*, 2013]. In contrast, *Uriarte and Papaik* [2007] suggested that downed trees incorporated into the soil enhance carbon sequestration by generating conditions favorable to tree growth in Southern New England forests. However, downed trees pose an increased fire risk with the potential to release carbon back into the atmosphere; although, forests will recover carbon lost in fires given a long enough regeneration period [*Kashian et al.*, 2006]. Even as the mechanical destruction of vegetation due to TC wind effects leads to short-term disturbances in healthy coastal forests, changes in vegetation activity and rainfall in tandem with the frequency of TC activity in Australia, particularly during drought periods, suggest that TC rainfall is important for soil water recharge during dry periods [*McGrath et al.*, 2012]. In the SE U.S., TC precipitation plays a critical role in restoring groundwater and soil moisture levels, thus facilitating drought recovery [*Brun and Barros,* 2013, 2014]. The positive impacts of TCs on terrestrial ecosystems by delivering large freshwater inputs during water stress periods are the focus of the present manuscript.

With an increasing likelihood of drought [*Sheffield and Wood*, 2007; *Meehl and Tebaldi*, 2004] and its adverse impacts on vegetation [*Vicente-Serrano et al.*, 2013; *Zhao and Running*, 2010], the water input that TCs provide is a significant fraction of the water cycle and important to sustain ecosystem function. Additionally, the SE U.S. contains the majority of temperate forests that play an important role in the U.S. carbon budget by acting as a carbon sink [*Anderson et al.*, 2010; *McKinley et al.*, 2011; *Sun et al.*, 2011]. Here we investigate the role TCs play on vegetation activity during recent wet and dry periods in the SE U.S. *Brun and Barros* [2014] evaluated the amount of water delivered to inland SE U.S. basins by TCs and linked the water input to storm timing and relative strength. For example, they showed that 2004 and 2005 would be dry years without the precipitation contribution from TCs. However, the contributions of TC precipitation in 2004 were higher than in 2005 due to more landfall events on the Atlantic Coastal Plains and trajectories through the Piedmont and along the Appalachian Mountains, whereas in 2005, there were largely Gulf Coast landfalls with continental tracks. In drought years (e.g., 2006 and 2007), the few landfalling TCs provided little additional precipitation in the watersheds away from the Coastal Plains. It is expected that the impact of TCs on GPP will vary based on antecedent moisture conditions, timing of TC landfall, and TC trajectory. The overall hypothesis of this study is twofold: (1) Atmospheric and soil conditions created by TCs have a positive impact on gross primary productivity (GPP) at the regional scale; and (2) TC impacts on GPP are modulated (amplified or damped) by hydrologic processes that determine the spatial and temporal variability of soil moisture along the storm path. The approach is to simulate plant photosynthesis and estimate GPP between 2002 and 2012 using the Duke Coupled Hydrology Model with Vegetation (DCHM-V) with realistic atmospheric forcing ("With" simulations) and upon

replacement of TC periods with climatology ("Without" simulations). We find carbon assimilation rates in the Piedmont and inner Appalachian Mountain region to be extremely sensitive to the timing and spatial distribution of rainfall provided by TCs, consistent with the physiographic organization of soil types and soil hydraulic properties, and the shallow regolith.

2. Methods

2.1. Model Description

The physics and dynamics of the DCHM-V are based on the 1-D land surface energy balance model originally implemented in *Barros* [1995] and described by *Devonec and Barros* [2002] that includes: (1) mass balance to solve for runoff, soil moisture, and soil temperature, (2) energy balance, and (3) snow accumulation and snowmelt physics. This model was later adapted into a 3-D distributed land hydrology model that includes surface-subsurface interactions [*Yildiz*, 2001], time-varying land use and land cover [*Yildiz and Barros*, 2007] and debris flows and slope failure [*Tao and Barros*, 2014a]. The model has been demonstrated to capture the hydrologic responses of different hydroclimatic regimes relying on ancillary data and without calibration at multiple timescales [*Devonec and Barros*, 2002; *Yildiz and Barros,* 2005, 2007, 2009; *Tao and Barros,* 2013, 2014a]. For this study, and based on prior experiments, the 1-D (column) implementation of the model is used where water and energy fluxes are evaluated at each pixel between the atmospheric boundary layer and three soil layers spanning 1 m of depth. Lateral routing of subsurface flows is not considered in the 1-D implementation, and low frequency processes are not explicitly represented (e.g., aquifer dynamics and deep water table fluctuations). Soil depths in complex terrain are shallow, and prior work in the Appalachian Mountains suggests that at 4 km resolution, 1 m soil depths are adequate to capture rainfall-runoff response and water storage [*Yildiz and Barros,* 2007, 2009]. The use of 1 m soil depths throughout the SE U.S. simulation domain is further supported by the presence of an impermeable layer of saprolite around 1 m of depth in the Piedmont [*Amoozegar et al.*, 1991]. In the Coastal Plain, soils are deeper and infiltration rates can be much higher than in the Piedmont, but the unconfined water table is shallow and soils are generally wet with precipitation exceeding evapotranspiration most of the year [*Eimers et al.*, 2001; *Markewich et al.,* 1990]. The model soil layers include a superficial layer and two deeper layers in the rooting zone. Each column represents the land surface as a single soil texture (selected based on the predominant soil type) and land cover class with its own surface roughness and soil hydraulic properties.

Garcia-Quijano and Barros [2005] integrated a photosynthesis model into the DCHM to represent vegetation processes as they relate to the water and energy balance. The description of photosynthesis within the DCHM-V is based on a biochemical formulation of leaf photosynthesis [*Farquhar et al.*, 1980; *Farquhar and von Caemmerer*, 1982; *Friend*, 1995] and the substrate structure dark respiration parameterization of *Thornley and Cannell* [2000]. The model captures well carbon assimilation, growing season timing, and soil vegetation-atmosphere interactions and feedbacks [*Garcia-Quijano and Barros*, 2005], as well as canopy-scale GPP [*Gebremichael and Barros*, 2006]. The regional aspect of this study requires modeling vegetation activity and response to hydroclimatic conditions across different plant functional types (PFTs). Thus, we use the photosynthesis model as described by *Garcia-Quijano and Barros* [2005] but modify the photosynthesis formulation to include temperature effects on photosynthetic responses and adapt the scaling from leaf- to canopy-level carbon assimilation to reflect individual plant type optical properties. These modifications are described in Supporting Information S1.

2.2. Data

2.2.1. Atmospheric Forcing Data

The DCHM-V was implemented without dynamic land-atmosphere coupling (i.e., "ran offline") at a 4 km spatial resolution and a 30 min time step, restrictions imposed by the inherent resolutions of the forcing data, and not the model. A comprehensive summary of forcing data sets is presented in Table S1 in the supporting information. The primary source for atmospheric forcing data is the North America Land Data Assimilation System Phase 2 (NLDAS-2), an integrated observation and model reanalysis data set designed to drive offline land surface models [*Mitchell et al.*, 2004; *Xia et al.*, 2012]. NLDAS-2 land surface forcing fields are derived from the North American Regional Reanalysis (NARR) fields and are available at 12.5 km spatial resolution and hourly and monthly temporal resolutions. Specific details on the spatial interpolation and temporal

disaggregation methods adopted in NLDAS-2 are described by *Cosgrove et al.* [2003]. All atmospheric variables are derived from NLDAS-2 except for precipitation. Due to the coarse spatial resolution, NLDAS-2 precipitation accumulations tend to be lower than observations and many spatial features of rainfall are lost [*Villarini et al.*, 2011]. Instead, we use Stage IV precipitation, a merged rain gauge-radar product at 4 km spatial and hourly temporal resolutions that can be obtained from the National Oceanic and Atmospheric Administration (NOAA) National Centers for Environmental Prediction (NCEP) [*Baldwin and Mitchell*, 1998; *Lin and Mitchell*, 2005]. Despite problems in mountainous regions [e.g., *Tao and Barros*, 2013], Stage IV captures well heavy rainfall accumulations and precipitation extremes due to its finer spatial and temporal resolution as compared to other data sets [*Villarini et al.*, 2011; *Nogueira and Barros,* 2015]. While the NLDAS-2 data have records since 1979, the Stage IV data are only available starting from 2002 limiting the start date for model simulations. NLDAS-2 field variables were bilinearly interpolated to the 4 km spatial grid used here, and both the field variables and Stage IV precipitation were linearly interpolated to a 30 min temporal resolution.

2.2.2. Ancillary Data

A combination of time-varying and static data sets and look-up tables (LUTs) were used to describe vegetation, soil, and land characteristics within the DCHM-V. All data are formatted to the 4 km spatial grid using a bilinear interpolation method for field variables and a nearest neighbor algorithm for all categorical data. Time-varying data are linearly interpolated to 30 min time intervals.

The vegetation phenology metrics of fraction of photosynthetically active radiation (FPAR) between 400 and 700 nm and leaf area index (LAI) were obtained from the Moderate Resolution Imaging Spectroradiometer (MODIS) Terra (MOD15A2) and combined Terra and Aqua (MCD15A2) data products [*Land Processes Distributed Active Archive Center*, 2006]. These data sets are available at 1 km spatial resolution and 8 day temporal resolution in a sinusoidal projection. The data were reprojected to a Lambert Conformal Conic (LCC) projection using the MODIS Reprojection Tool (MRT) [*Dwyer and Schmidt*, 2006]. In order to quality control, fill gaps and reduce noise in the time series data, an adaptive Savitzky-Golay filter using TIMESAT was used [*Jönsson and Eklundh*, 2004]. The Savitzky-Golay filter, a weighted moving average performed as a convolution, smooths time series data with a polynomial least squares fit that preserves higher moments in the data and reduces bias introduced from applying the filter [*Chen et al.*, 2004]. This filter was applied successfully to MODIS LAI data previously [e.g., *Yuan et al.*, 2011; *Tao and Barros*, 2014b].

Land surface albedo and vegetation fraction were acquired from the NLDAS-2 Mosaic Land Surface Model L4 data set at hourly temporal resolution and 0.125° by 0.125° spatial resolution [*Xia et al.*, 2012]. This data set provides land surface parameters simulated from the Mosaic land surface model where individual subgrid vegetation tiles perform an energy and water balance [*Koster and Suarez,* 1994, 1996].

The MODIS Land Cover Type product (MCD12Q1) provided information on biome type. Based on the MODIS land cover classification, a LUT (look-up table) was compiled from the NLDAS Mapped Static Vegetation Data (http://ldas.gsfc.nasa.gov/nldas/web/web.veg.table.html), the Weather Research and Forecasting (WRF) Land Use Table [*Michalakes et al.*, 2001], and *Manzoni et al.* [2011] to determine model parameters such as minimum canopy resistance, roughness length, and critical leaf water potential, respectively. Specifically, the University of Maryland (UMD) classification scheme was used for its large number of distinct land cover types (i.e., no mosaic bins). These data are available at 500 m resolution for each year between 2001 and 2012. The data were reprojected from a sinusoidal projection to LCC using MRT. In the DCHM-V, the land cover type is updated each year following the values provided by the MCD12Q1 data set. The vegetation parameters for roughness length, minimum canopy resistance, and critical leaf water potential are selected according to the biome type (Table S2).

Soil parameters were inferred from the Soil Information for Environmental Modeling and Ecosystem Management CONUS-SOIL Texture and Porosity data sets and LUTs with values for field capacity, wilting point, saturated hydraulic conductivity, pore size distribution, and wetting front soil suction head. CONUS-SOIL provides static map coverages of soil properties derived from the State Soil Geographic Database (STATSGO) [*Miller and White*, 1998]. Soil texture data are available at 500 m and soil porosity is available at 30 arcsec, both comprising 11 soil layers. Each grid cell is classified by taking the most common soil type and porosity across the eight soil layers representing 1 m of soil depth. Figure 1f shows the final soil texture classification for the SE U.S. Soil water retention and infiltration parameters are based on soil texture and follow *Rawls and Brakensiek* [1982] and *Rawls et al.* [1991, 1993] (Table S3).

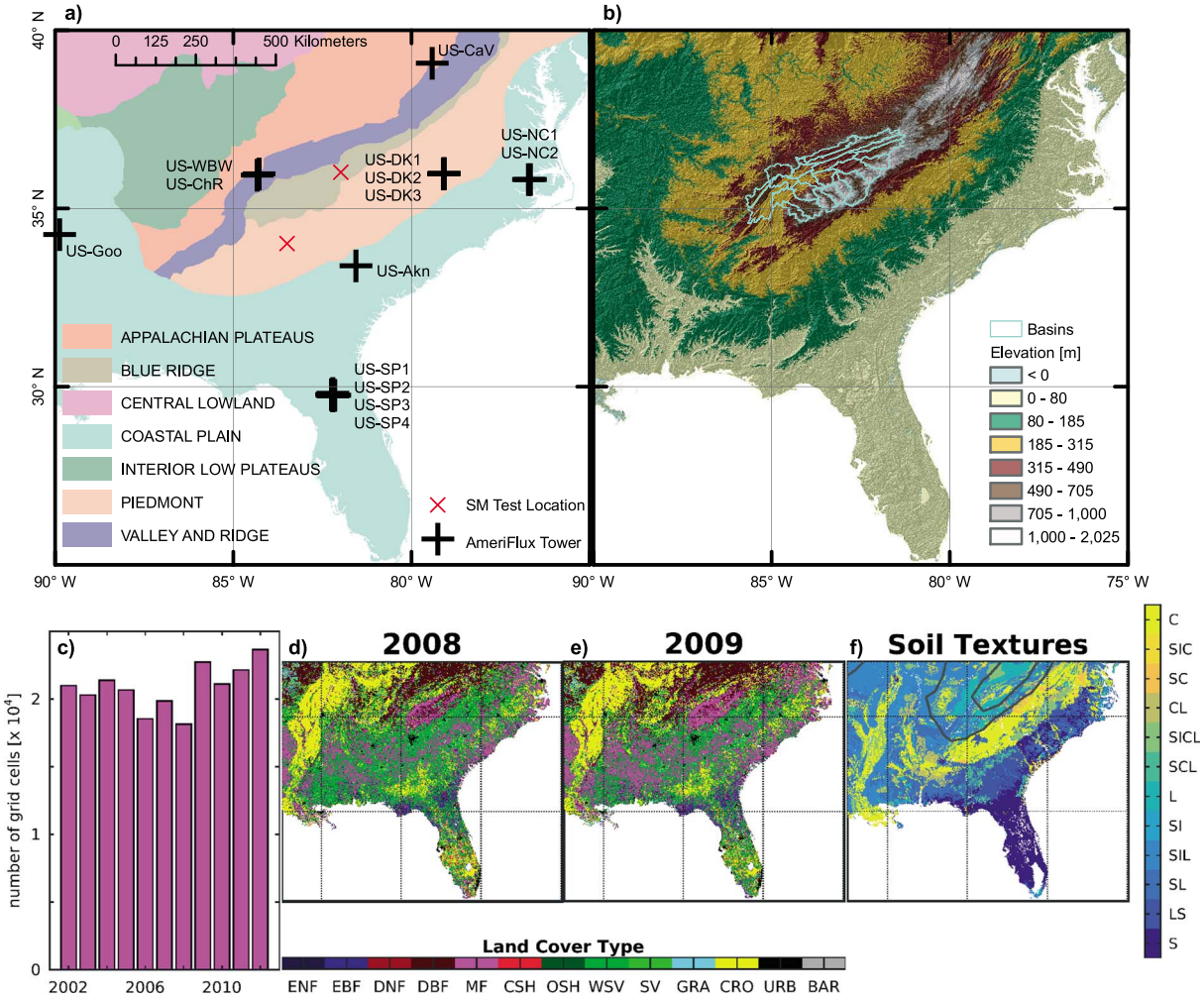

Figure 1. Maps of the study area and bar chart of mixed forest land cover change between 2002 and 2012 to demonstrate high spatial variability over complex terrain. (a) Map of AmeriFlux eddy covariance tower locations used in this study and two locations for soil moisture (SM) tests with the physiographic regions of the SE U.S. Physiographic divisions data set provided by the USGS (http://water.usgs.gov/GIS/metadata/usgswrd/XML/physio.xml). (b) Elevation map of SE U.S. (downloaded from USGS HydroSHEDS: http://hydrosheds.cr.usgs.gov/index.php) with high elevation basins determined from the USGS Hydrologic Units of the U.S. data set (http://water.usgs.gov/GIS/metadata/usgswrd/XML/huc250k.xml). (c) Bar chart of number of mixed forest (MF) 4 km pixels from the MODIS MCD12Q1 Land Cover data for 2002–2012. (d, e) Maps of MODIS Land Cover for 2008 and 2009. Full names for legend entries are listed in Table S2. (f) Map of soil textures soil depth from CONUS-SOIL database with 250 and 500 m elevation contours marked as gray lines. Each pixel is classified by taking the most common soil type across eight soil layers representing 1 m of soil depth. Full names for legend entries are listed in Table S3. Lines of latitude and longitude are the same in all maps.

2.2.3. CO_2 Flux Data

The DCHM-V simulated GPP is compared to tower-based GPP from AmeriFlux eddy covariance towers and the satellite-derived GPP product from MODIS to evaluate the model's ability to capture carbon cycle features of specific biomes in the SE U.S. The model runs were conducted at 30 min time steps over the period 2002–2012 to estimate GPP at each tower location. Extended gaps, lack of temporal consistency, and uncertainty in the meteorological data at the towers lead us to use the forcing data described in section 2.2.1 as instrument calibration and tower maintenance may vary in time and introduce uncertainties that are difficult to quantify [*MacDonald*, 1972]. The AmeriFlux data provide half-hourly measurements of CO_2 flux or net ecosystem exchange (NEE; CO_2 flux corrected for storage) and cover a range of vegetation types and physiographic regions in the SE U.S. [*Baldocchi*, 2003; *Baldocchi et al.*, 2001] (Table 1 and Figure 1). When available we use site-provided GPP estimated from NEE measurements and carbon balance principles (Table 1). As these data are not available for all towers or all years of the simulation, the DCHM-V results were also compared to the MODIS data. The MODIS MOD17A2 GPP product is available at 1 km spatial resolution as 8 day composites. The MOD17 algorithm follows *Monteith* [1972] by assuming that net primary productivity

Table 1. Summary of AmeriFlux (AMF) Towers[a]

Site ID	Site Name	Latitude	Longitude	Elevation [m]	AMF Vegetation Type	Years of Data Available	References
US-Akn	Aiken	33.3833	−81.5656	92	MF	2011–2013	
US-CaV	Canaan Valley	39.0633	−79.4208	994	GRA	2004–2010	
US-ChR	Chestnut Ridge	35.9311	−84.3324	286	DBF	2005–2010	
US-DK1	Duke Forest-open field	35.9712	−79.0934	168	GRA	2001–2008	*Stoy et al.* [2006]
US-DK2	Duke Forest-hardwoods	35.9736	−79.1004	168	DBF	2001–2008	*Pataki and Oren* [2003]
US-DK3	Duke Forest-loblolly pine	35.9782	−79.0942	163	ENF	1998–2008	*Oren et al.* [1998, 2006]
US-Goo	Goodwin Creek	34.2547	−89.8735	87	GRA	2002–2006	*Gilmanov et al.* [2010]
US-NC1	NC Clearcut	35.8118	−76.7119	5	ENF	2005–2009	
US-NC2	NC Loblolly Plantation	35.8030	−76.6685	5	ENF	2005–2010	*Noormets et al.* [2010]
US-SP1	Slashpine-Austin Cary	29.7381	−82.2188	50	ENF	2000–2011	*Clark et al.* [2004]
US-SP2	Slashpine-Mize	29.7648	−82.2448	50	ENF	1999–2008	*Clark et al.* [2004]
US-SP3	Slashpine-Donaldson	29.7548	−82.1633	50	ENF	1999–2010	*Clark et al.* [2004]
US-SP4	Slashpine-Rayonier	29.8028	−82.2032	47	ENF	1998	
US-WBW	Walker Branch Watershed	35.9588	−84.2874	283	DBF	1995–2007	

[a]DBF, deciduous broadleaf forest; ENF, evergreen needleleaf forest; GRA, grasslands; and MF, mixed forest.

(NPP) under nonstressed conditions and during the growing season is linearly related to the amount of absorbed photosynthetically active radiation (APAR). This method of calculating GPP differs from the biochemical formulation of the DCHM-V, as a light-use efficiency parameter stands in for the variability across vegetation types in converting APAR into usable plant energy [*Heinsch et al.*, 2003; *Running et al.*, 2000, 2004]. In general, MODIS tends to overestimate GPP by 20–30% compared to tower data, specifically underestimating springtime GPP because of early leaf onset but overestimating midsummer GPP due to insufficient drought constraints [*Heinsch et al.*, 2006*; Running et al.*, 2004]. Additionally, the MOD17 algorithm does not capture well rapid changes in phenology over short timescales [*Verma et al.*, 2014].

Comparison against AmeriFlux tower data allowed us to assess the DCHM-V's ability to reproduce carbon cycle characteristics of distinct contiguous U.S. ecoregions [*Hargrove et al.*, 2003]. Due to discontinuities and the local nature of the flux tower data, MODIS GPP is used for comparison as well for its ability to reproduce documented spatial and temporal variability for different biomes [*Heinsch et al.*, 2006]. Challenges arise when comparing GPP estimates from flux towers, satellite observations, and model output [*Verma et al.*, 2014]. Each data source has its own implicit spatial scale for which GPP estimates are valid. In the case of flux towers, the associated spatial scale is the footprint of the tower, which varies depending on wind direction and surrounding heterogeneous land cover [*Baldocchi*, 1997]. Thus, the representative spatial scale of the tower data may vary in time depending upon upwind conditions and tends to change in size with boundary layer conditions (i.e., strength of vertical fluxes). Further, flux tower GPP estimates depend on estimates of maintenance respiration which show large errors during nocturnal periods and across seasons [e.g., *Baldocchi*, 2003; *Lai et al.*, 2002; *Goulden et al.*, 1996] and cannot distinguish between autotrophic and heterotrophic respiration and anthropogenic emissions [e.g., *Running et al.*, 2004; *Falge et al.*, 2002]. MODIS data and the DCHM-V provide gridded representations where estimated GPP is an integrated value over the grid cell extent. In both the MOD17A2 product and the DCHM-V results, homogeneous land cover is assumed for each grid cell, neglecting subgrid scale heterogeneity in vegetation types.

2.3. Experimental Setup

2.3.1. With Simulations

The DCHM-V is forced with the same atmospheric and ancillary data described in section 2.2 during the control simulations with TC activity (hereafter, With simulations). The model runs were conducted at 30 min time steps over the period 2002–2012. In this study, water and energy fluxes are evaluated separately for each pixel. Without computing lateral flow routing, we expect an underestimation of soil moisture in alluvial valleys as interflow and subsurface flow play a dominant role in distributing water after large rainfall events at high spatial resolution in the mountains [*Tao and Barros,* 2013, 2014a].

2.3.2. Without Simulations

In the modified model runs without TC activity (hereafter, Without simulations), we use a reduced forcing where atmospheric fields during active TC periods are replaced with the climatological average for the same days of the year. The climatology itself was calculated from the control atmospheric forcing data, but omitting periods of TC landfall and trajectory in the SE U.S. (Table 2 and Figure S1). Discontinuities between the

Table 2. Impact of Landfalling TCs in the SE U.S. Between 2004 and 2007[a]

Year	Name	Landfall Date	Exit Date	% Area Impacted	Total ΔGPP (Mg C/m^2)
2004	Bonnie	11 August	13 August	17	+0.13
2004	Charley	13 August	15 August	17	+0.16
2004	Gaston	27 August	31 August	22	+0.19
2004	Frances	3 September	9 September	24	+0.41
2004	Ivan	15 September	18 September	19	+0.27
2004	Jeanne	25 September	28 September	13	+0.21
2004	Matthew	10 October	11 October	11	+0.09
2005	Arlene	11 June	12 June	11	+0.07
2005	Cindy	5 July	8 July	18	+0.15
2005	Dennis	9 July	13 July	20	+0.24
2005	Katrina	25 August	30 August	28	+0.33
2005	Rita	20 September	26 September	26	+0.29
2005	Tammy	5 October	7 October	23	+0.16
2005	Wilma	24 October	25 October	5	+0.03
2006	Alberto	12 June	14 June	8	+0.05
2006	Ernesto	30 August	1 September	12	+0.10
2007	Barry	1 June	4 June	13	+0.08
2007	Gabrielle	9 September	10 September	8	+0.04
2007	Humberto	13 September	14 September	12	+0.06

[a] Δ = With − Without

control forcing and the climatology without TCs are avoided by using a weighted average between the data sets over a 3 day transition period before and after TC landfall (Figure 2). The weights for the climatology and control forcing range from 0 to 1, the sum of which always equals 1. Over the 3 day transition period before TC landfall, the weights for the normal forcing decrease from 1 to 0 and the weights for the climatology increase from 0 to 1. During the TC landfall period, the weight for the climatology is 1 and for the control forcing is 0. In the 3 day transition period following TC exit from the domain, the reverse occurs.

We focus the analysis of results on the two periods of interest: (1) wet years 2004–2005 with high numbers of TC tracks over land and (2) drought years 2006–2007. Removing the signature of TCs from the forcing data reduces precipitation accumulations across the SE U.S. (Figure 3). Annual precipitation totals are significantly higher along storm tracks in the wet years (2004 and 2005) and slightly higher in the dry years, except for 2006 when one TC delivered a large amount of precipitation to the Carolinas compared to the climatological average.

2.3.3. Simulation Conditions

The key coupling mechanism between carbon assimilation rates and the water and energy budget is the stomatal conductance [*Garcia-Quijano and Barros*, 2005]. Stomatal conductance describes the ease with which water vapor is released from plant stomata in the leaves to the atmosphere. This plant function is controlled by temperature, solar radiation, soil moisture, and the vapor pressure deficit. Aside from precipitation, the other atmospheric states and fluxes that will impact the stomatal conductance function and influence GPP estimates by the DCHM-V are temperature, specific humidity, and incoming solar radiation. Replacing periods of TC landfall in the atmospheric forcing data with the climatological mean impacts these other data sets as well. In the reduced forcing data used in the Without simulations, surface temperature along the TC tracks tends to be cooler in the midsummer and warmer in the fall season. In general, the incoming shortwave radiation tends to be higher in the Without simulations along the TC tracks, but slightly cloudier conditions appear away from the TC

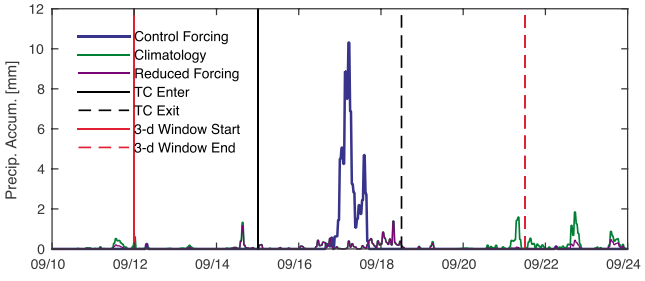

Figure 2. Example of how the atmospheric data sets are prepared for the With and Without TC simulations. Illustration of the atmospheric data products described in the flowchart in Figure S1: (1) Precipitation forcing data during Hurricane Ivan (2004) used in the With Simulation (blue); (2) Climatology for each 30 min period over 10–25 September (green); and (3) the Reduced forcing precipitation data between 10 and 25 September 2004 used in the Without Simulation (indigo).

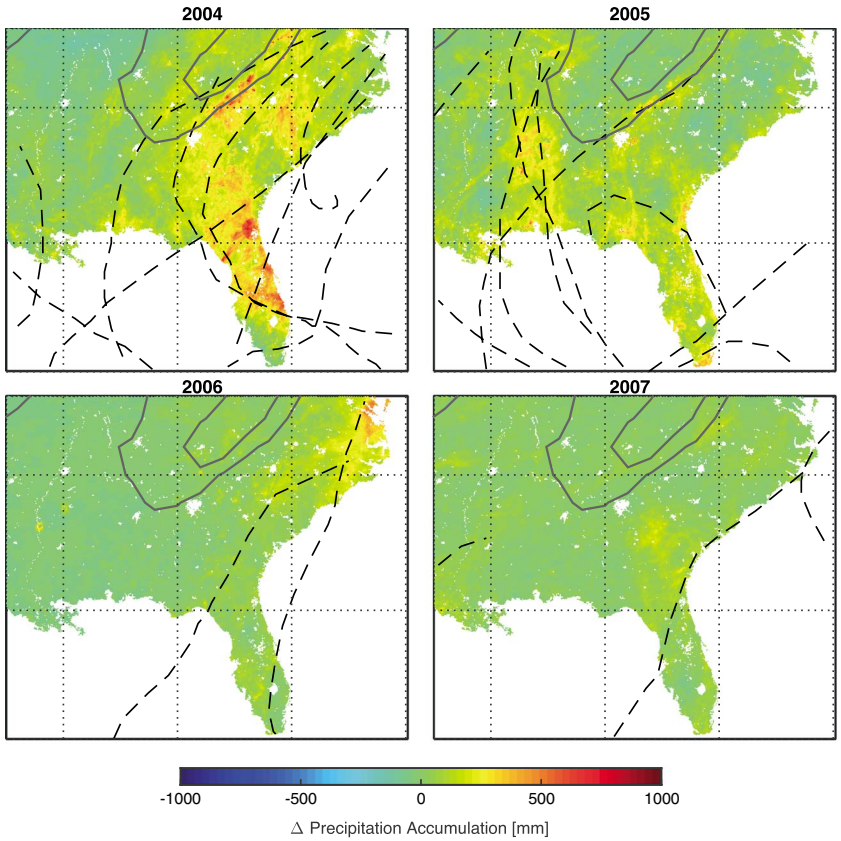

Figure 3. Difference between annual precipitation accumulations in the With and Without simulations between 2004 and 2007 (Δ = With − Without). Warm colors indicate higher values in the With simulation forcing and cool colors indicate higher values in the Without simulations. TC storm tracks are displayed as dashed black lines. The gray lines indicate the 250 m and 500 m elevation contours. Urban areas and large water bodies are removed from analysis and displayed in white. We observe areas with higher values in the Without simulations as a result of the systematic replacement of TC periods with the climatological averages to a small extent. This results in the overestimation of precipitation in areas not impacted by landfalling TCs in the Without simulations as demonstrated by the area west of the Appalachian Mountains in 2004 and the eastern Carolinas in 2005. Lines of latitude and longitude are the same as in Figure 1.

tracks. This is an artifact of replacing the forcing over the entire domain. The Without simulations are also less humid than the With during the TC periods.

The Appalachian Mountains and Piedmont are regions of complex terrain with high spatial and temporal variability in land cover. Annual land cover types from the MODIS MCD12Q1 product used to force the DCHM-V (Figures 1d and 1e) show that, in general, there is little change in vegetation types in the region over the 11 simulation years except for a decrease in the spatial extent of mixed forest and increase in savannas and shrub lands over the mountains during drought years (2006–2008) (Figure 1c). Soil types play a role in how different physiographic regions respond to TC precipitation because of the large range of soil textures present in the study area. Inspection of soil texture classifications maps (Figure 1f) indicates that the Piedmont region is predominantly composed of shallow clayey soils with low infiltration rates and porosity, and hydraulic and hydrologic behavior that is highly sensitive to drought. Infiltration and saturated hydraulic conductivity rates are low in this region and typical of clay soils [*Buol and Weed*, 1991; *Markewich et al.*, 1990; *Amoozegar et al.*, 1991].

3. Results

3.1. Evaluation at AmeriFlux Tower Sites

The DCHM-V captures well the phenology and amplitude of vegetation activity across the different vegetation types as compared to the AmeriFlux tower data and MODIS GPP product (Figures 4 and S2). The

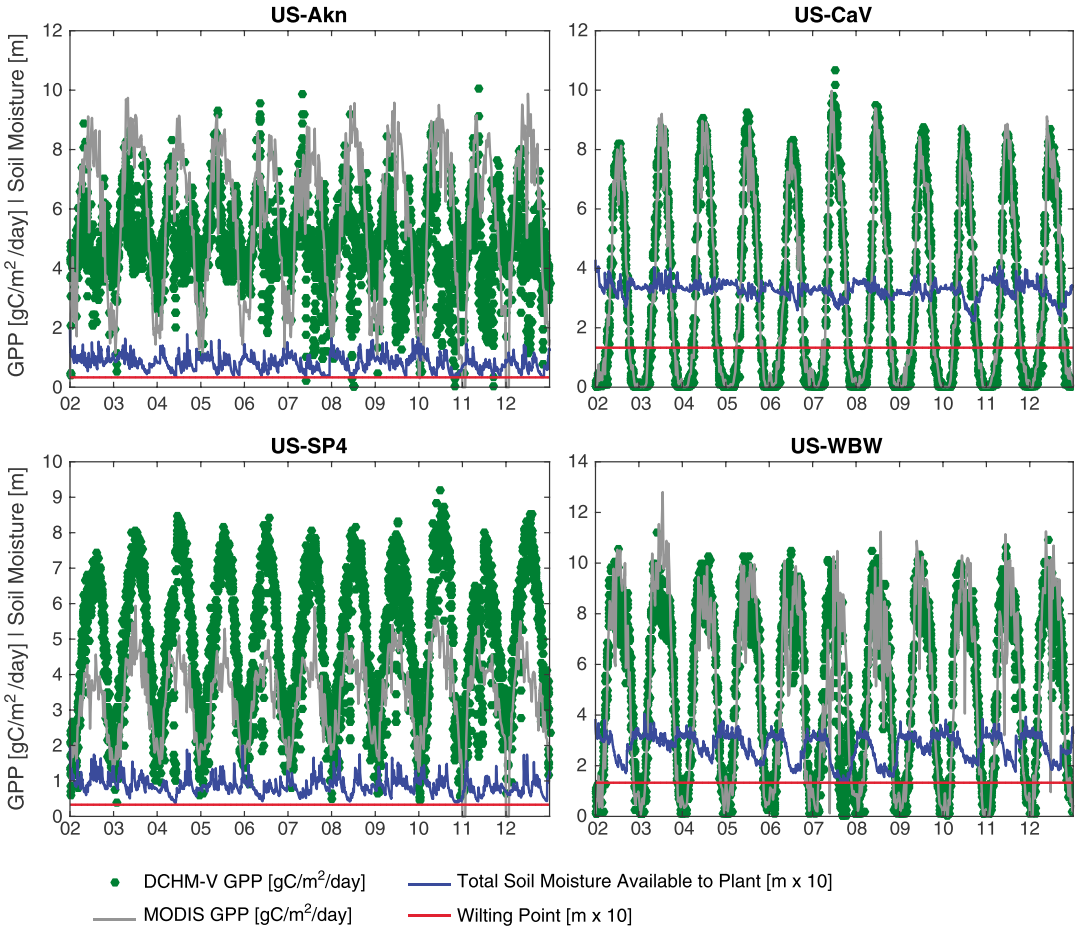

Figure 4. Time series of daily average GPP estimates and column soil moisture (blue) estimated by the DCHM-V. MODIS GPP is plotted in gray and the wilting point is displayed in red. Four different cases demonstrate the impact of water availability on GPP estimates from the DCHM-V and how it influences deviations from the MODIS GPP product. At the US-Akn site soil moisture is consistently near wilting point, placing the vegetation under water stress. Water limitation does not restrict GPP at the US-CaV tower. The US-SP4 site estimates from the DCHM-V are much higher compared to MODIS due to the MODIS GPP algorithm and not the availability of water at this location. The US-WBW tower demonstrates the impact of the 2007 drought where GPP is reduced because of limited soil water availability.

close agreement in the seasonality of vegetation activity between the DCHM-V and MODIS is expected because we use the MODIS FPAR and LAI products as phenology indicators within the model. For consistency with these model inputs, the vegetation parameters are specified according to the MODIS land cover type classification rather than the vegetation type provided by the AmeriFlux tower site information. Aside from the noted discordance in scale, this difference in representation of vegetation explains much of the discrepancy between the DCHM-V and AmeriFlux tower comparisons as MODIS pixels often have completely different land cover types specified for the 4 km grid within which the towers sites reside (Tables 1 and 3). For example, the US-NC2 site is classified as cropland in the MODIS land cover data, but as evergreen needleleaf forest in the AmeriFlux data. If the PFT is changed to reflect the classification at the AmeriFlux tower in the DCHM-V simulations, the relative error between the two decreases by 0.34 g C/m^2/d (not shown).

Noted differences in the amplitude of seasonal GPP signal between MODIS and DCHM-V occur at the US-Akn and the US-SP4 tower sites. The overestimation of MODIS GPP compared to the DCHM-V at the US-Akn tower is attributed to the lack of water stress constraints in the MODIS algorithm. The soil moisture at the tower is consistently near wilting point, resulting in lower GPP estimates from the DCHM-V during the midsummer (Figure 4). On the other hand, the underestimation of MODIS GPP at the US-SP4 tower location is not related to water availability. Instead, the MODIS FPAR and LAI products for this tower are considerably lower than what the tower measured (maximum FPAR ~ 0.75; maximum LAI ~ 3). The

Table 3. Summary of GPP Estimates From DCHM-V at SE U.S. AmeriFlux Tower Locations[a]

Site ID	MODIS Vegetation Type	Mean Annual GPP [g C/m^2/yr]	Daily Maximum GPP [g C/m^2/d]	RMSD (DCHM-V vs AMF) [g C/m^2/d]	RMSD (DCHM-V vs MODIS) [g C/m^2/d]	RMSD when SM > FC (DCHM-V vs MODIS) [g C/m^2/d]
US-Akn	MF	1741	10.0	--	2.72	2.42
US-CaV	DBF	1131	10.7	--	0.57	0.54
US-ChR	DBF	1871	11.5	--	1.76	0.90
US-DK1	WSV	1221	11.2	1.42	2.20	1.05
US-DK2	DBF	1736	11.1	1.38	1.97	0.92
US-DK3	DBF	1736	11.1	1.41	1.97	0.92
US-Goo	WSV	1266	9.6	1.37	1.35	1.00
US-NC1	MF	1855	10.2	--	1.58	1.51
US-NC2	CRO	1120	9.4	2.35	2.20	2.19
US-SP1	WSV	2326	11.7	2.47	2.83	2.35
US-SP2	WSV	2326	11.7	1.47	2.83	2.35
US-SP3	WSV	2305	11.4	1.45	2.73	2.33
US-SP4	WSV	1783	9.2	--	2.02	2.16
US-WBW	DBF	1827	11.2	--	1.63	0.76

[a]RMSD = root-mean-square difference. Calculated using daily GPP estimates from RMSD $= \sqrt{\frac{\sum_{i=1}^{n}(\mathrm{est}_i - \mathrm{obs}_i)^2}{n}}$. SM, soil moisture; FC, field capacity; DBF, deciduous broadleaf forest; ENF, evergreen needleleaf forest; GRA, grasslands; MF, mixed forest; and WSV, woody savannas.

MODIS algorithm depends directly on FPAR and LAI [*Running et al.*, 2000]; thus, the MODIS GPP is heavily influenced by the low FPAR and LAI values for this tower.

The impact of water stress is evident at all of the towers except US-CaV (Figure 4). At the US-CaV site, soil moisture remains considerably above the wilting point, and we observe no drop in GPP due to water stress. Results for US-WBW illustrate well the impact of water limitation on GPP during drought periods. In Figure 4, the effect of the 2007 drought on vegetation activity is demonstrated through the limited photosynthesis at the US-WBW tower. Similar constraints on photosynthesis in 2007 can be seen at the US-ChR and Duke flux tower sites (US-DK1, US-DK2, and US-DK3; Figure S2).

Where AmeriFlux GPP estimates are available, the DCHM-V estimates carry small relative errors (Table 3). The root-mean-square difference (RMSD) between the DCHM-V GPP and eddy covariance data is less than 1.5 g C/m^2/d for all tower sites except for US-NC2 and US-SP1. This suggests that the standard deviation in the difference between the two GPP estimates at each tower location is within the standard error for the tower estimates themselves [*Goulden et al.*, 1996; *Baldocchi*, 2003; *Oren et al.*, 2006; *Desai et al.*, 2008]. The short record length at the US-NC2 tower and the discontinuous nature of the US-SP1 data may play a role in the larger RMSD values. Additionally, incongruences in vegetation classification in the model and at the tower sites for both of these locations explain higher RMSDs.

The GPP estimates from the DCHM-V fall within the range reported in the peer-reviewed literature. At each tower location, daily maximum GPP estimated by the DCHM-V ranges from 9 to 12 g C/m^2/d. In general, the highest daily maximum values estimated by eddy covariance flux towers are around 14 g C/m^2/d for deciduous and evergreen forests, while the lowest values fall near 8 g C/m^2/d for grasslands [*Luo et al.*, 2001; *Richardson et al.*, 2009]. The annual average GPP estimates from the DCHM-V also show good agreement with previously observed values. Grassland GPP estimates tend to be at the lower end of the range for photosynthetic activity, typically between 626 and 1313 g C/m^2/yr and prairie estimates as high as 1383 g C/m^2/yr [*Ma et al.*, 2007; *Tian et al.*, 2010]. The US-Goo, US-NC2, and US-DK1 sites all fall within this range (Table 3). Note that the estimates from *Ma et al.* [2007] are for a Mediterranean climate, which tends to be dryer than the SE U.S., and GPP typically correlates with precipitation amount at the annual timescale [*Ma et al.*, 2007]. A wide range in GPP estimates exists for evergreen forests with the largest value reported by *Tian et al.* [2010] at 2584 g C/m^2/yr for the Duke Forest. This is much higher than the DCHM-V simulated value for the Duke Forest site, and the other forest sites (US-CaV, US-ChR, and US-WBW) all fall below this amount. Duke Forest DCHM-V GPP estimates fall within the range of values derived from flux tower measurements [*Stoy et al.*, 2006; *Schäfer et al.*, 2003; *Luo et al.*, 2001; *Hamilton et al.*, 2002; *Lai et al.*, 2002; *Tian et al.*, 2010]. Note that vegetation age may also impact carbon assimilation and vegetation activity [*Grant et al.*, 2010], but this is not accounted for.

3.2. Sensitivity of SE U.S. GPP to TC Forcing 2002–2012

3.2.1. With Simulations

The annual average GPP for the SE U.S. from the DCHM-V and MODIS shows a similar spatial pattern of relatively high GPP along the coastlines and low GPP in the croplands surrounding the Mississippi river (Figures S3 and S4). In the DCHM-V, the Piedmont and inner mountain region have relatively low GPP compared to the rest of the SE U.S., but in the MODIS GPP there is no noticeable trend along the complex terrain or to reflect the contrasting geomorphology and soil hydraulic properties between the Piedmont and the Coastal Plains.

Directly comparing GPP from MODIS and the DCHM-V shows the large difference in the inner Appalachian Mountains and Piedmont regions. MODIS estimates much higher GPP, while the DCHM-V estimates lower assimilation rates in these areas (Figure 5). This underestimation of GPP in the mountains and foothills results from low soil water availability that creates water stress and lowers transpiration rates in the DCHM-V simulations. The effect of water stress is evident in the annual maps of latent heat flux estimated for the same period in the model (Figure 6). Little water is available in the soils for evapotranspiration, resulting in the low GPP estimates in the Piedmont and mountain regions. The soil water stress impact is even more pronounced during drought years (2006–2008).

To better understand the seasonal variation in GPP estimated by the DCHM-V we consider the wet year 2005 (Figure 7). Water stress does not impact vegetation activity in the mountain and Piedmont regions until the peak of summer (July) and persists until regional vegetation activity becomes dormant (October). This effect is partially attributable to the underestimation of precipitation by the Stage IV data over complex terrain. As the Stage IV product is derived from radar, ground clutter is a problem along the foothills and steep terrain of the Appalachians, while the inner mountain region is completely invisible to the radar [*Prat and Barros*, 2010a]. Further, few of the gauges used for correcting radar precipitation estimates are located at high elevations, resulting in severe underestimation of rainfall in this region [*Prat and Barros*, 2010a; *Tao and Barros*, 2013]. A continuous underestimation of precipitation by Stage IV combined with higher temperatures and solar radiative forcing during the warm season create conditions for higher evaporation rates from soils starting in July and results in the model's underestimation of GPP through the end of summer and into the fall. Until the water stress, created by the intersection of underestimated precipitation input and high evaporative demand of the warm season, becomes apparent, the DCHM-V matches MODIS GPP well and even estimates higher GPP in the Coastal Plain and Interior Lowland Plateaus during the "greening up" period (Figure 8).

The DCHM-V GPP estimates are highly sensitive to fluctuations in water input, consistent with expected theoretical and experimental behavior [*Garcia-Quijano and Barros*, 2005]. Low transpiration rates reflect water stress conditions created in the model when precipitation rates are low and temperature is high. While the decrease in carbon assimilation rates in response to soil water stress conditions in the Appalachian Mountain and Piedmont regions may be overestimated, especially because lateral flow redistribution can alleviate the soil moisture deficit, the sensitivity demonstrated by the model suggests an aptitude for investigating the impact of removing TCs from the atmospheric forcing data sets.

3.2.2. Comparisons Between With and Without Simulations

3.2.2.1. Seasonal Timescale

The influence of TC number and trajectories is demonstrated in the differences in GPP estimates between the With and Without simulations during the warm season (Figure 9). We only present values of the change in daily average GPP that are greater than 1 g C/m^2/d to account for the uncertainty in the reduced atmospheric forcing data.

In the years with high TC activity (2004 and 2005), there is a significant increase in GPP (Δ = With − Without) around the eye tracks when TCs are present, as high as 4–6 g C/m^2/d in some areas (Figure 9). Almost all landfalling TCs during the 2004 hurricane season follow tracks along the Appalachian Mountains and the East Coast, and GPP increases in the Inner Mountain and Piedmont regions. In the Piedmont alone, 1.35 Mg C/m^2 can be attributed to TC activity in 2004 (Table 4). (Note that in this article the units Mg C/m^2 correspond to a sum of fluxes for all pixels rather than an average flux. These are different interpretations and to reduce confusion with regards to the units the values should be multiplied by the domain grid cell area (16 sq. km) to obtain a cumulative mass.) On the other hand, hurricane landfalls occurred preferentially along the Gulf Coast with trajectories to the west of the Appalachian Mountains in the inner continental region in 2005. The largest increases in GPP in 2005 occur in the region that includes the Interior Lowland Plateaus, Appalachian Plateaus, and Coastal Plains.

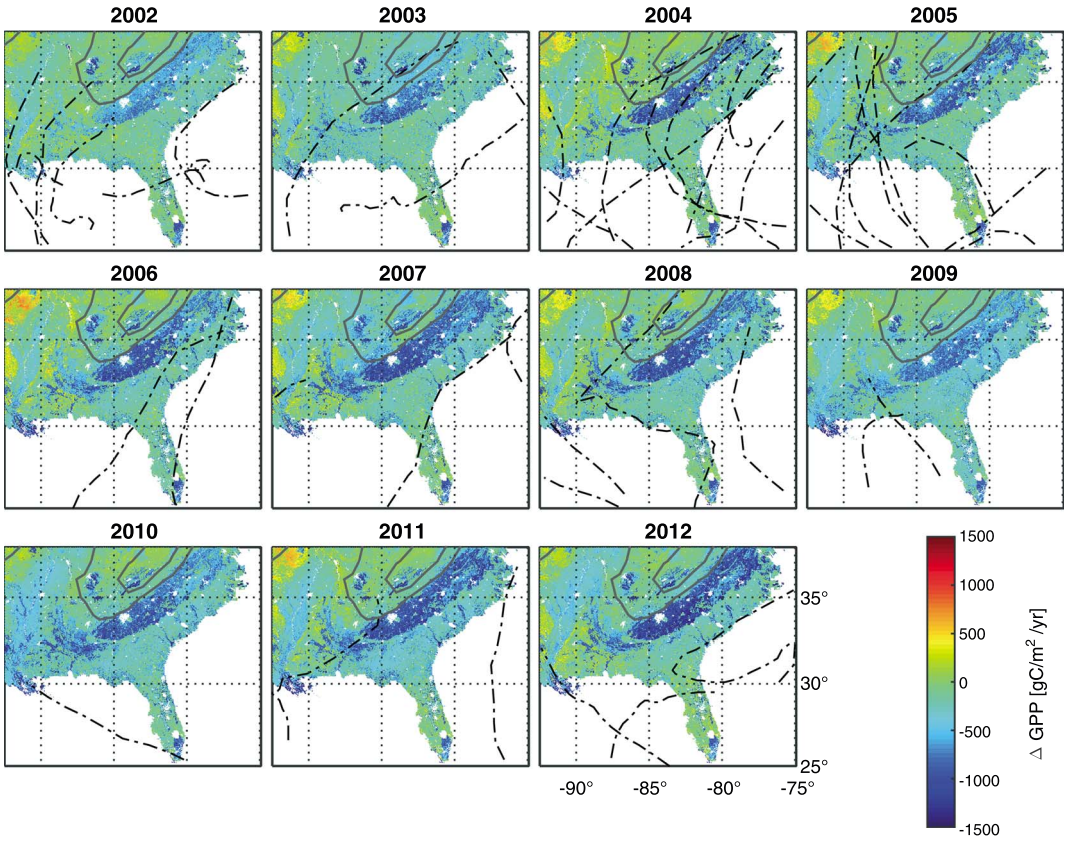

Figure 5. Absolute difference between annual GPP from the DCHM-V With simulation and MODIS (Δ = DCHM-V − MODIS). Warm colors indicate that the DCHM-V GPP is higher and cool colors indicate that the MODIS GPP is higher. TC storm tracks are displayed as dashed black lines. The gray lines indicate the 250 m and 500 m elevation contours. Urban areas and large water bodies are removed from analysis and displayed in white.

More than half of total change in GPP associated with TCs in 2005 is located in the Coastal Plains, with 2.68 Mg C/m^2 assimilated in this region alone (Table 4). Orographic enhancement of rain from Hurricane Cindy and Tropical Storm Tammy allows for increases in GPP in the Piedmont (Figure 9 and Table 4). The 2005 wet season has a higher cumulative change in GPP associated with the presence of TCs because they impact over 50% of the SE U.S. domain. The 2004 TCs impact almost 40% of the SE U.S., with most of the total change in GPP occurring in the Piedmont region through which many of the eye tracks passed (Table 4). A noticeable difference between the two wet years is the magnitude of average daily GPP during TC passage (Figure 9). This is related to the antecedent rainfall conditions for each year. Without the precipitation from TCs, most of the region would have experienced severe meteorological and hydrological drought, whereas non-TC precipitation is higher in 2005 [*Brun and Barros*, 2014]. In both years, the GPP differential that can be directly attributed to TC activity is ~9% of the total warm season carbon assimilated in areas impacted by TCs. That total is 32.9 Mg C/m^2 in 2004 and 53.5 Mg C/m^2 in 2005. Thus, an average productivity in the 3–5 Mg C/m^2 range can be attributed to TC activity in wet years in the SE U.S.

During drought years (2006 and 2007), local and modest increases in GPP (Δ = With − Without) reflect the small number of TCs and the low precipitation amounts delivered by these storms, on the order of 1–2 g C/m^2/d (Figure 9). Note that this change is within the range of model uncertainty. The two landfalling TCs in 2006 delivered rainfall to the Carolinas (~200 mm in Figure 3) and increased GPP nearby in the Piedmont. The 2007 storms produced very small rainfall accumulations in the SE U.S., demonstrated in the low GPP increases, and small aerial extent impacted (Table 4). The net change in GPP over the Piedmont is markedly different between the two drought years. The 2006 hurricane season allows for 0.65 Mg C/m^2 to be assimilated in this physiographic region, while the 2007 season is associated with less than a quarter of that amount. Further, 8.2% of the total warm season GPP in areas impacted by TCs is associated with the two landfalling TCs in 2006 (total GPP is

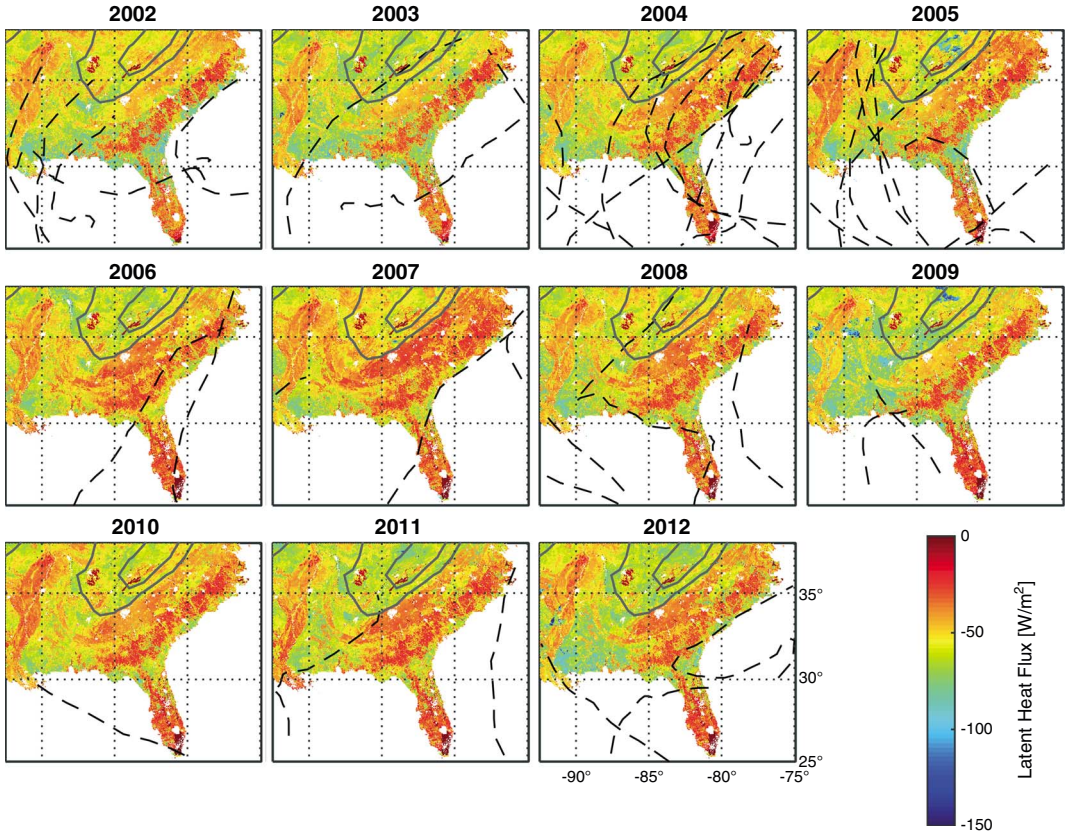

Figure 6. Annual average latent heat flux estimated by the DCHM-V With simulations over the SE U.S. Negative values indicate fluxes out of the land surface and into the boundary layer. TC storm tracks are displayed as dashed black lines. The gray lines indicate the 250 m and 500 m elevation contours. Urban areas and large water bodies are removed from analysis and displayed in white.

17.0 Mg C/m^2). In contrast, the percentage in 2007 is only 4% of the 35.2 Mg C/m^2 assimilated by vegetation in areas impacted by TCs. Details on individual storms are provided below.

3.2.2.2. Storm-Scale Impacts

In 2004, the seven landfalling TCs are associated with an increase in GPP along the Appalachian Mountains and Piedmont region (Figure 10). Bonnie was a tropical storm at landfall that produced only modest amounts of rainfall, around 1–4% of annual precipitation, across the Atlantic Coast states. Hurricane Charley arrived immediately after and produced similar patterns in rainfall accumulations, with slightly larger fractions of annual precipitation totals in the Carolinas [*Brun and Barros*, 2014]. Both storms are associated with an increase in GPP in the Piedmont, with larger increases from Hurricane Charley in the Carolinas. Gaston made landfall in South Carolina as a H1 category hurricane and had a limited impact on GPP located in a narrow band west of eye track in the coastal plains but increasing GPP by as much as 35 g C/m^2. The first large hurricane of 2004, Frances, contributed to over 20% of the annual mean precipitation in the Piedmont and Blue Ridge [*Brun and Barros*, 2014], resulting in modest increases in GPP in the mountains, but large increases in the Piedmont (between 10 and 60 g C/m^2). Hurricane Ivan was another large storm with an inland track along the Southern Appalachians, whose environmental impacts (i.e., debris flows and landslides) were enhanced by the antecedent soil moisture conditions provided by Hurricane Frances [*Wooten et al.*, 2007]. This storm is also associated with the large increases in GPP and a widespread area of impact in the SE U.S. (Table 2). This increase is pronounced over the Piedmont and Valley and Ridge physiographic regions at around 10–30 g C/m^2 (Figure 10). Hurricane Jeanne produced heavy rainfall along its eye track in the Piedmont and the impact on GPP is similar to Hurricane Ivan in space but smaller in magnitude. Finally, Tropical Storm Matthew produced strong rains east of its track resulting in small increases in GPP across the SE U.S. The total increase in GPP associated with each storm over the region is displayed in Table 2. The largest storms in terms of spatial impact induce the largest increases in GPP, with Hurricane Frances alone associated with an increase of 0.41 Mg C/m^2 over the entire SE U.S. domain.

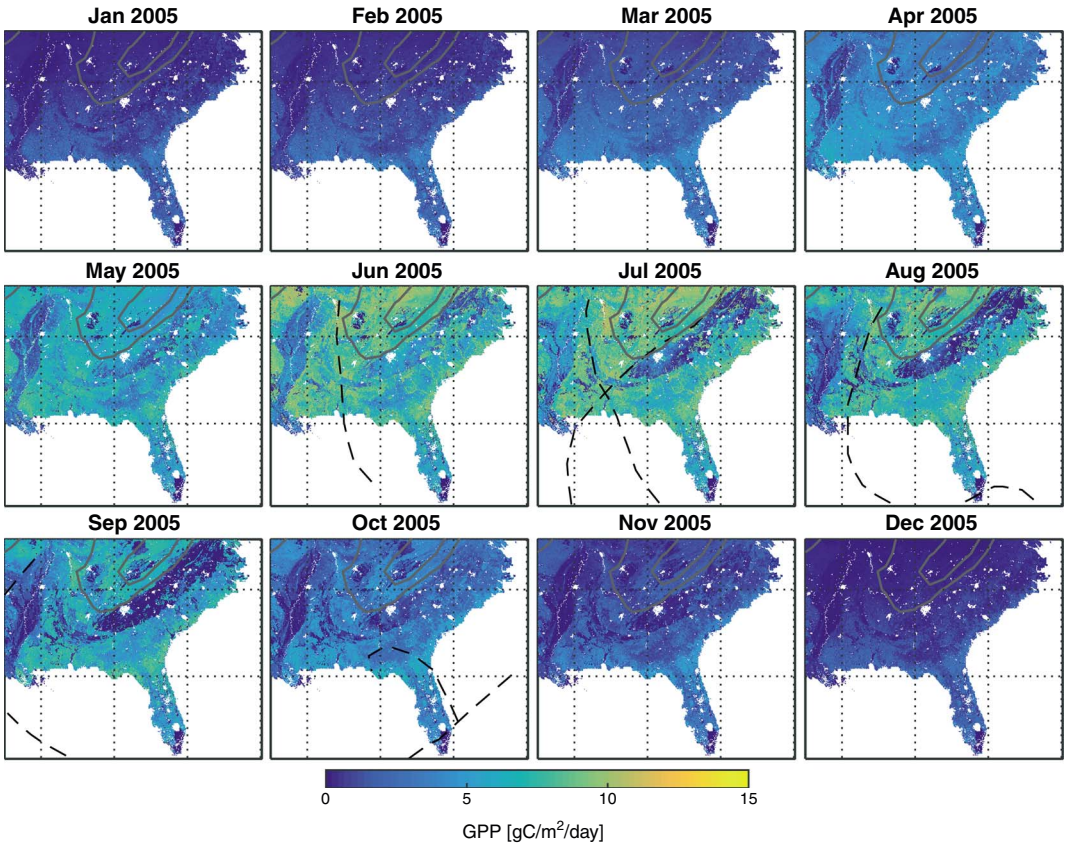

Figure 7. Average daily GPP for each month in 2005 estimated by the DCHM-V With simulations. TC storm tracks are displayed as dashed black lines. The gray lines indicate the 250 m and 500 m elevation contours. Urban areas and large water bodies are removed from analysis and displayed in white. Lines of latitude and longitude are the same as in Figure 1.

The 2005 storms resulted in smaller increases in GPP compared to those in 2004 but tended to impact larger areas (Figure 11 and Table 2). A large spatial extent in the SE U.S. received moderate precipitation accumulations from Tropical Storm Arlene and Hurricane Cindy; however, their timing during the peak summer season allowed for increases in GPP in regions where photosynthesis is water limited. Hurricane Dennis also arrived in the peak of summer and produced precipitation far from its track in Georgia from a large leading cloud shield [*Brun and Barros*, 2014]. The impact on GPP is evident around Atlanta and near the eye track. While Hurricane Katrina was associated with large rainfall amounts at landfall, its overall contribution to the annual rainfall total was less than 6% across the SE U.S. and at most 16% close to the track [*Brun and Barros*, 2014]. Consequently, the associated increases in GPP are clustered near the track with some values as high as 35 g C/m^2. Hurricane Rita contributed almost 20% of the annual precipitation in Louisiana, increasing GPP over a small extent in Louisiana and Alabama. The heavy precipitation produced by Tropical Storm Tammy in the Piedmont is consistent with orographic enhancement and small increases in GPP are associated with this effect. Finally, while Wilma was an intense hurricane at landfall, its short track located in southern Florida limited its impact on regional GPP. Because 2005 had higher rainfall totals without the contribution from TCs than 2004, smaller increases in GPP were associated with individual storms across the SE U.S. However, the 2005 storms impacted larger areas and their cumulative impact on the entire SE U.S. domain is higher at around 0.24–0.33 Mg C/m^2 for Hurricanes Dennis, Katrina, and Rita (Table 2).

During the dry years (2006 and 2007), very low annual precipitation amounts led to severe drought conditions over the SE U.S. The 2006 storms Alberto and Ernesto were relatively weak and had modest impacts on GPP regionally (Table 2). Tropical Storm Alberto lost its convective organization shortly after landfall and weakened to a tropical depression over South Carolina [*Franklin and Brown*, 2008]. Tropical Storm Alberto had a moderate impact on GPP along the Piedmont and in the Blue Ridge due to the low rainfall

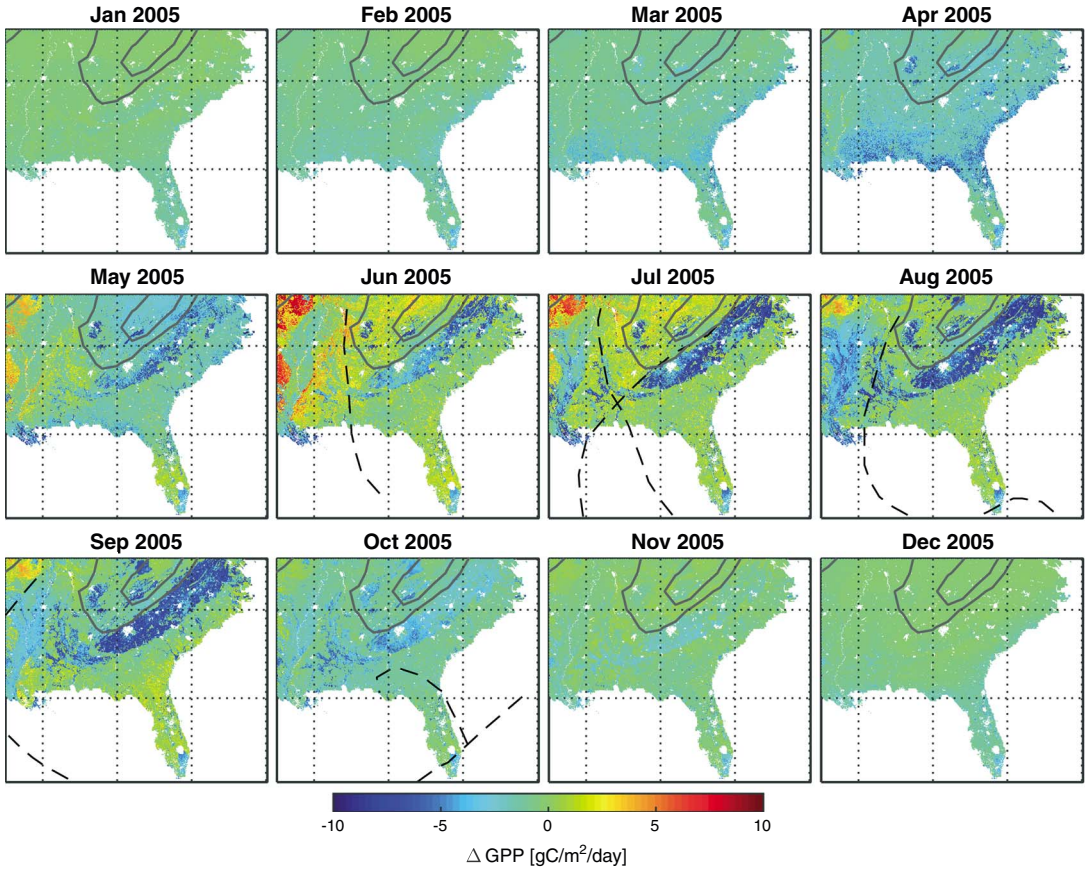

Figure 8. Difference in the average daily GPP for each month in 2005 over the SE U.S. estimated by the DCHM-V With simulations and MODIS (Δ = DCHM-V − MODIS). Warm colors indicate higher values in the DCHM-V and cool colors indicate higher values in the MODIS product. TC storm tracks are displayed as dashed black lines. The gray lines indicate the 250 m and 500 m elevation contours. Urban areas and large water bodies are removed from analysis and displayed in white. Lines of latitude and longitude are the same as in Figure 1.

totals preceding landfall (0.05 Mg C/m^2). Hurricane Ernesto made landfall in Florida and North Carolina as a tropical storm and produced heavy rainfall over the Carolinas, Virginia, and southern Maryland. As a stronger storm, Hurricane Ernesto impacted a larger area with modest increases in GPP in the Piedmont (10 g C/m^2) and across the entire domain (0.10 Mg C/m^2). The three landfalling TCs in 2007 followed very different paths with limited impacts on regional GPP. Tropical Storm Barry increased precipitation in Florida and Georgia, resulting in small, localized increases in GPP totaling 0.08 Mg C/m^2. While Tropical Storm Gabrielle made landfall along the Cape Lookout National Seashore, convection remained offshore, leading to the lowest increases in GPP in the SE U.S. associated with a TC (Table 2). The heaviest rains associated with Hurricane Humberto occurred in Texas and Louisiana, with the storm dissipating over Mississippi [*Brennan et al.*, 2009]. The small changes in GPP over the western portion of the study domain are associated with the small increases in rain provided by the remnants of this storm, which have an impact due to the dry conditions over the region. Thus, in drought years with weak TC activity, the benefits of TC precipitation are still significant though only at local scales.

4. Discussion

4.1. Precipitation Forcing

High-quality precipitation data at appropriate spatial and temporal resolution are essential to force hydrologic models and capture realistic rainfall-runoff response as well as soil moisture dynamics. This particularly includes the diurnal cycle of precipitation. The Stage IV precipitation product provides reasonable estimates over noncomplex terrain at hourly time-scales, but it severely underestimates rainfall intensity in the

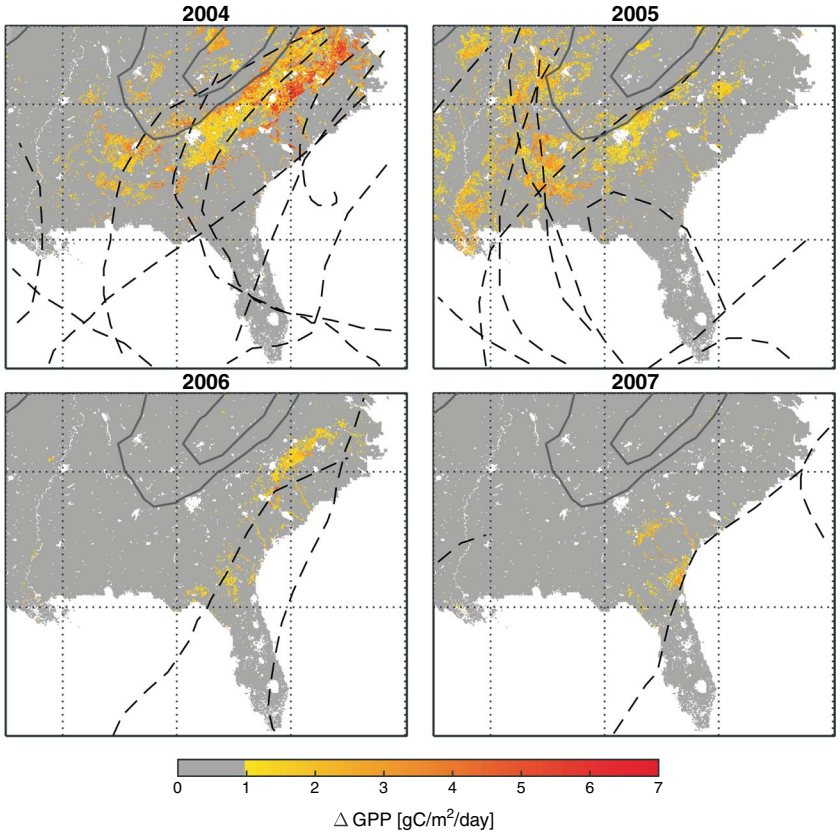

Figure 9. Difference between daily average DCHM-V GPP estimates over the wet seasons in 2004–2007 in the With and Without simulations (Δ = With − Without). The wet season is defined as 15 April to 15 October. TC storm tracks are displayed as dashed black lines. The gray lines indicate the 250 m and 500 m elevation contours. Urban areas and large water bodies are removed from analysis and displayed in white. Values of Δ less than 1 g C/m^2/d are considered within the range of uncertainty of the precipitation data. Lines of latitude and longitude are the same as in Figure 1.

Appalachian Mountains, and even more so within the inner mountain region due to radar blocking by the terrain and the lack of rain gauges for bias correction [e.g., *Tao and Barros*, 2013; *Prat and Barros*, 2010a]. This impacts soil moisture in the DCHM-V and the GPP estimates for this area. In contrast, the MODIS algorithm does not account for the subdiurnal hydrology of these regions and does not exhibit the same sensitivity to the water stress conditions.

Additional considerations regarding precipitation in the high-elevation areas of the domain include light rainfall and cloud and fog immersion, which dominate the diurnal cycle of precipitation in the cold season and play an important role in modulating the spatial variability of precipitation at lower elevations, including the reverse orographic enhancement effect identified by *Wilson and Barros* [2014, 2015]. These conditions are not captured by radar or by the operational rain gauges. *Johnson and Smith* [2006] reported that spruce-fir forests in the Appalachian Mountains experienced such conditions nearly 70% of time during the growing season and identified foliar uptake as a preferred mode of water use by trees. *Berry and Smith* [2013b] further showed that foliar uptake by spruce-fir saplings native to high elevations (above 1500 m) in the Southern Appalachians led to increases in leaf water content of 3.7 to 6.4%. While condensed water on leaves has the potential to limit CO_2 uptake, the authors found cloud immersion contributes to improved water status and foliar uptake without inhibiting CO_2 uptake. In greenhouse experiments of a species native to cloud forests in Brazil, *Eller et al.* [2013] observed a novel mechanism where water absorbed directly through the leaves was redistributed through the xylem to other plant tissues. This suggests that making a modest correction to the precipitation data over the inner mountain region will diminish the strong soil water stress signal demonstrated in our results.

Table 4. Cumulative Impact of Landfalling TCs During the Wet Season (15 April to 15 October) in the SE U.S. Between 2004 and 2007[a]

Year	# of TCs	Total Area Impacted [%]	Total ΔGPP [Mg C/m^2]	AP Area Impacted [%]	AP ΔGPP [Mg C/m^2]	BR Area Impacted [%]	BR ΔGPP [Mg C/m^2]	CP Area Impacted [%]	CP ΔGPP [Mg C/m^2]	IP Area Impacted [%]	IP ΔGPP [Mg C/m^2]	PM Area Impacted [%]	PM ΔGPP [Mg C/m^2]	VR Area Impacted [%]	VR ΔGPP [Mg C/m^2]
2004	7	39.3	+2.9	40.3	+0.28	39.9	+0.16	43.2	+0.83	47.9	+0.10	73.4	+1.35	47.3	+0.20
2005	7	52.0	+4.9	64.6	+0.30	88.4	+0.11	54.5	+2.68	77.3	+0.62	79.7	+0.84	68.4	+0.17
2006	2	22.7	+1.4	25.4	+0.02	37.7	+0.07	21.4	+0.39	22.2	+0.02	66.1	+0.65	43.9	+0.09
2007	3	33.8	+1.4	53.8	+0.10	86.0	+0.10	32.4	+0.86	31.3	+0.06	66.6	+0.17	67.3	+0.09

[a]Δ = With − Without; AP, Appalachian Plateaus; BR, Blue Ridge; CP, Coastal Plains; IP, Interior Lowland Plateaus; PM, Piedmont; and VR, Valley and Ridge.

To explore the potential impact of light rainfall, we made a simple correction to the Stage IV precipitation data to account for fog and light rainfall in the inner mountain region defined by basins in Figure 1b. The correction distributes 0.5 mm of rainfall over a 3 h period (11 A.M.–2 P.M.) during the warm season (April–October) consistent with the climatology of rainfall from the Duke rain gauge network in the Pigeon river basin [*Prat and Barros,* 2010a, 2010b; *Wilson and Barros*, 2014; *Duan et al.*, 2015]. A new experimental DCHM-V With simulation was repeated using the precipitation forcing with light rainfall correction. Low-level clouds and fog have a significant impact on the radiative forcing and light availability; however, in this experiment no corrections to the incoming shortwave and longwave radiation were applied due to the lack of a robust quantitative estimate. Under cloud immersion, photosynthetically active radiation (PAR) becomes less variable throughout the day and leaves are exposed to diffuse and optimal PAR for longer lengths of time [*Johnson and Smith*, 2006]. Additionally, lower temperatures and near-zero vapor pressure deficit (VPD) means lower transpiration costs [*Berry and Smith*, 2013b]. This implies that even if the diurnal cycle of rainfall is improved in these exploratory simulations, the low-level climate is too warm, surface temperatures are too high, and thus, evapotranspiration is overestimated and GPP impacts are underestimated. The greatest change in simulated GPP occurs in areas with clay soil texture with the largest differences around 2–3 g C/m^2/d during the peak summer months (Figure 12). We see a small increase in photosynthesis by simply making more water available to the plants; however, cloud immersion improves leaf-level carbon assimilation rates by altering the forest microclimate in addition to increasing water input. Field experiments in the Southern Appalachian spruce-fir forests show increased afternoon leaf-level photosynthesis rates and leaf conductance on cloud-immersed days compared to clear days during the growing season [*Berry and Smith*, 2013a]. Transpiration demand is high in clear days in the morning leading to lower xylem water potentials and partial stomatal closure by the afternoon. Thus, we expect our simple experiment to underestimate carbon assimilation rates in the presence of fog and low-level clouds due to these additional changes in microclimate that provide more favorable conditions for plant photosynthesis. Further comprehensive observations of local microclimates are necessary to understand and improve quantitative estimates of water use and carbon uptake in SE U.S. mountain forests.

4.2. Impact of Soil Moisture Stress on GPP

The high sensitivity of the DCHM-V simulations to water stress conditions as compared to MODIS estimates is not only demonstrated in Figures 5 and 8 but also apparent in the relationship between GPP and LAI. Model GPP estimates do not scale linearly with LAI and instead show diminishing increases in GPP with higher LAI (Figure 13), a result of implementing Beer's law to scale from leaf- to canopy-scale carbon assimilation rates. The water limitation imposed by the model hydrology is demonstrated in how the relationship between GPP and LAI changes with soil texture. In particular, clay-rich soils show smaller GPP increases with LAI compared to other soil types. The lack of sensitivity to water stress in the MODIS algorithm results in GPP estimates that do not capture well the beginning and end of the growing season, as well as abrupt changes in CO_2 fluxes caused by water limitations, and is well documented in the literature [*Álvarez-Taboada et al.*, 2015; *Zhang et al.*, 2015; *Verma et al.*, 2014; *Gebremichael and Barros*, 2006; *Turner et al.*, 2003].

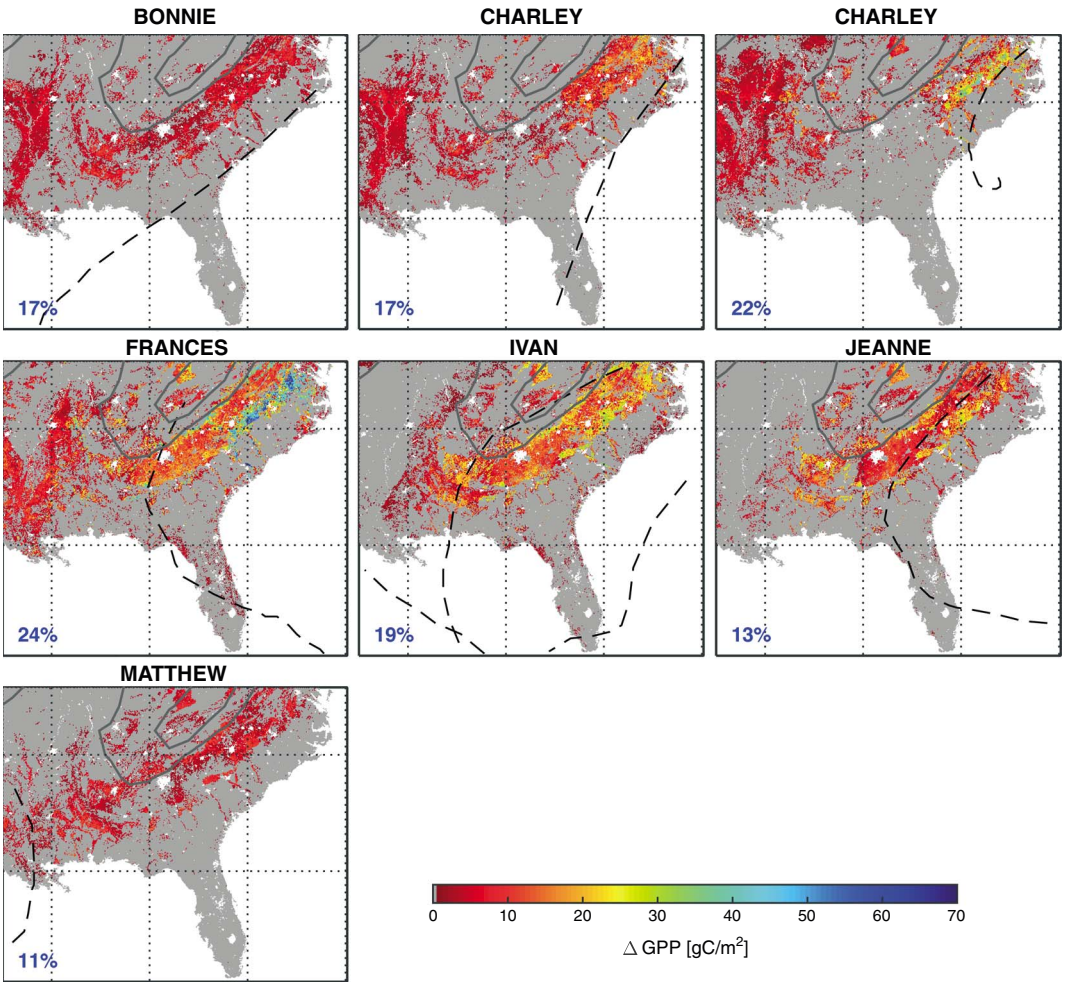

Figure 10. Cumulative difference between GPP estimates over individual TC landfall periods in 2004 (Δ = With − Without). TC storm tracks are displayed as dashed black lines. The gray lines indicate the 250 m and 500 m elevation contours. Urban areas and large water bodies are removed from analysis and displayed in white. The portion of the SE US domain impacted by TC landfall is displayed as a percentage in blue. Lines of latitude and longitude are the same as in Figure 1.

The low GPP estimates from the DCHM-V over the Piedmont and inner mountain region are directly linked to soil texture and water stress. This issue is further illustrated by contrasting the sensitivity to soil moisture conditions in two grid cells within the SE US domain, one in the Blue Ridge region and another in the Piedmont (Figure 1a). Specifically, two idealized simulations were conducted with soil moisture fixed at field capacity and at saturation, and a third simulation was conducted by converting clayey soils to sandy soils. At both grid locations the potential GPP estimated by the DCHM-V for both ideal soil water conditions matches MODIS well as expected because plant water availability is never limited (Figure 14). Further, in the With model simulations, estimated GPP matches MODIS well through the greening-up period and then declines in the peak summer months. This effect is more pronounced in the Piedmont pixel with clay soil texture, in agreement with the larger Piedmont area where the DCHM-V estimates low GPP throughout the summer months. Note that if the soil texture is changed to sand, the DCHM-V estimates GPP closer to MODIS (Figure 14). The change in soil texture implies change in soil hydraulic properties and therefore soil moisture dynamics. It is clear that the soil hydraulic properties are exerting a large control on water available to plants, and Piedmont clay soils are responsible for the low GPP estimates in the DCHM-V, an effect that is not captured by the MODIS product. Model results differ from MODIS (i.e., $\Delta GPP > 1$ g C/m^2/d) in over 90% of the Piedmont physiographic region, and the DCHM-V GPP estimates are 53% lower in wet years and 60–67% lower in dry years.

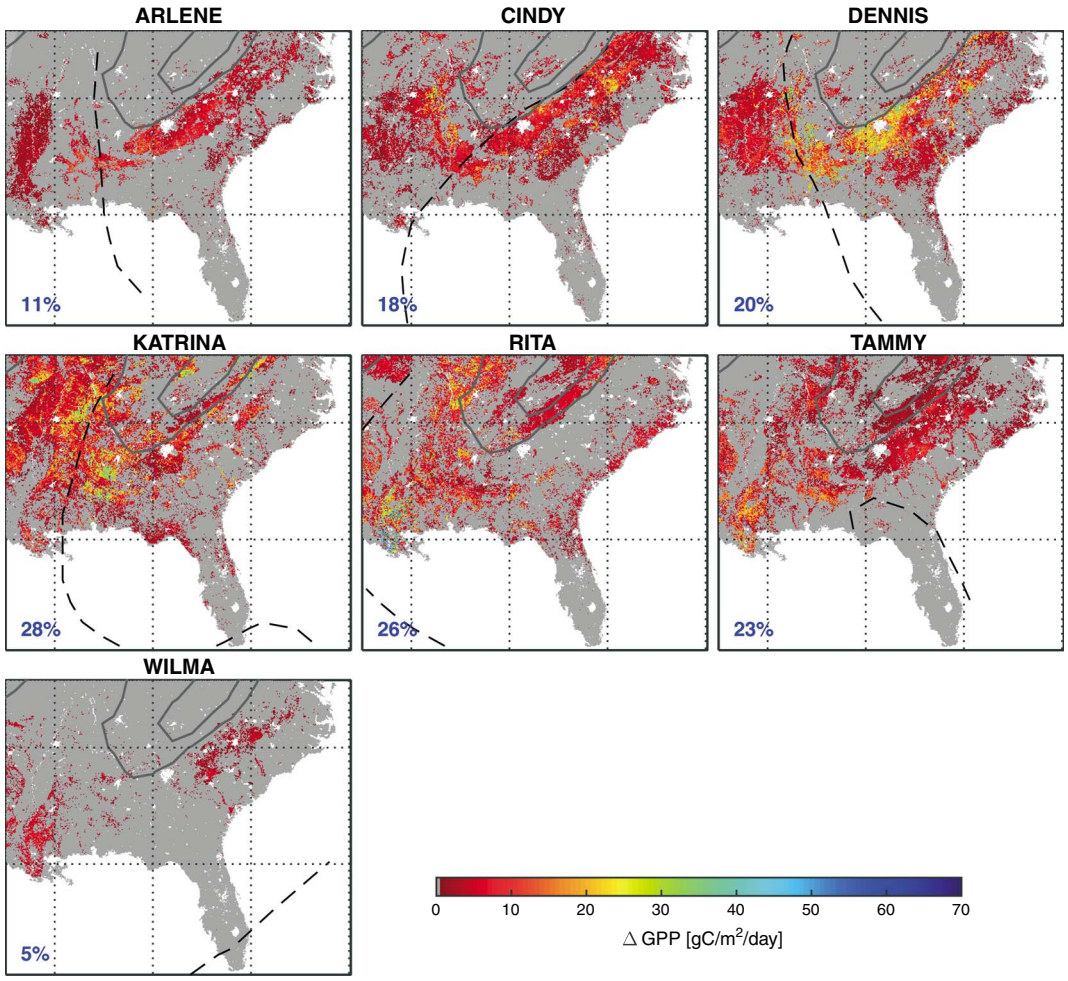

Figure 11. Cumulative difference between GPP estimates over individual TC landfall periods in 2005 (Δ = With − Without). TC storm tracks are displayed as dashed black lines. The gray lines indicate the 250 m and 500 m elevation contours. Urban areas and large water bodies are removed from analysis and displayed in white. The portion of the SE U.S. domain impacted by TC landfall is displayed as a percentage in blue. Lines of latitude and longitude are the same as in Figure 1.

Shallow roots implicit in the model configuration play a role in limiting water available for uptake in the soils. *Amoozegar et al.* [1991] report roots commonly occurring at 1 m depth in the Piedmont. These roots would have access to water stored at the nearly impermeable boundary demarcated by the saprolite [*Buol and Weed*, 1991], which is not captured here, and thus, water stress may be overestimated in the model especially in the case of trees with deeper roots. Nevertheless, the DCHM-V spatial patterns of low GPP in the Piedmont region are consistent with decreasing NPP and ET attributed to drought conditions in other studies [e.g., *Tian et al.*, 2010].

4.3. Scaling TC Precipitation With GPP and Soil Moisture

Previous studies demonstrate a linear relationship between precipitation and GPP at the annual timescale [e.g., *Ma et al.*, 2007]. However, we observe a change in variance when TCs produce less rainfall over the SE U.S. (Figure 15a). The wet years (2004 and 2005) show higher sensitivity to additional precipitation (~2 g C/m^2/d higher in With simulations across the year) compared to the dry years. Across the two wet years there is a notable difference in how the mountain basins, areas with high water stress in our simulations, respond to the TC precipitation. Recall that 2004 is a dryer year without the precipitation associated with TCs than 2005. In Figure 15a, we see more spread in how these grid cells respond to the TC precipitation in 2004, whereas in 2005 additional precipitation has a smaller impact on water stress areas.

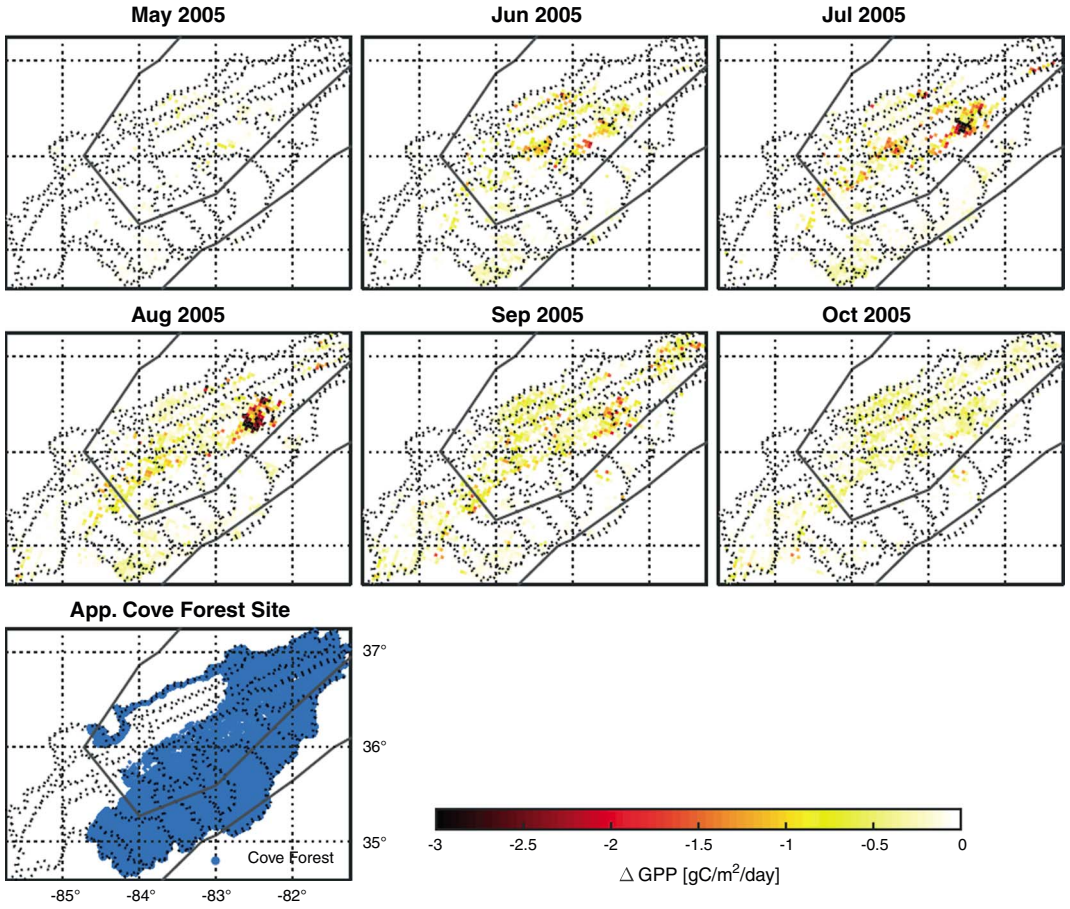

Figure 12. Difference in daily average GPP between control simulation and light rainfall experiment between May and October over the inner mountain domain during the wet year 2005 (Δ = With − "Light Rainfall"). (bottom) The locations of Appalachian Cove Forests, which have high species richness and require moist conditions. Basin boundaries are marked in black dashed lines (see Figure 1b). The 250 m and 500 m elevation contours are marked as solid gray lines.

The relationship between precipitation and soil moisture is also highly varied across the domain. Again, when TCs provide a large freshwater input at the basin scale, the impact on soil moisture is greater (Figure 15b). The same differences between wet and dry years and between the two wet years noted in the previous paragraph are relevant here. The scatter in 2006 reflects the areas in the Carolinas that did receive a significant precipitation input by Ernesto.

4.4. Considerations for Canopy Resistance and Implications

Change in shortwave radiation between the With and Without simulations had a small impact on GPP ($\Delta GPP < 1\ g\ C/m^2/d$ for nearly all pixels in the study domain) with no clear relationship between the two variables (not shown). There is also no clear relationship between the change in temperature and GPP from the DCHM-V simulation results. However, the procedure for creating a Without TC data set for shortwave radiation and temperature is not as rigorous as the precipitation data set because of the large uncertainty in cloud cover distribution, and there are not enough data to make a careful sensitivity study for these forcing variables. This work's findings suggest that changes in precipitation are keys to altering GPP. This is in agreement with prior studies that suggest mutual constraints between carbon and water fluxes. Specifically, they find carbon sequestration is influenced by water availability and decreases during drought periods [e.g., *Tian et al.*, 2010; *Sun et al.*, 2011], and spatial patterns of carbon uptake tend to follow precipitation patterns in the SE U.S. [*Tian et al.*, 2010].

4.5. TC Timing and Eye Track Trajectory

The impact that TCs have on GPP depends on how they move through the domain (trajectory) and at which point in the year they arrive (timing). In 2004, the landfalling TCs arrive late in the hurricane season

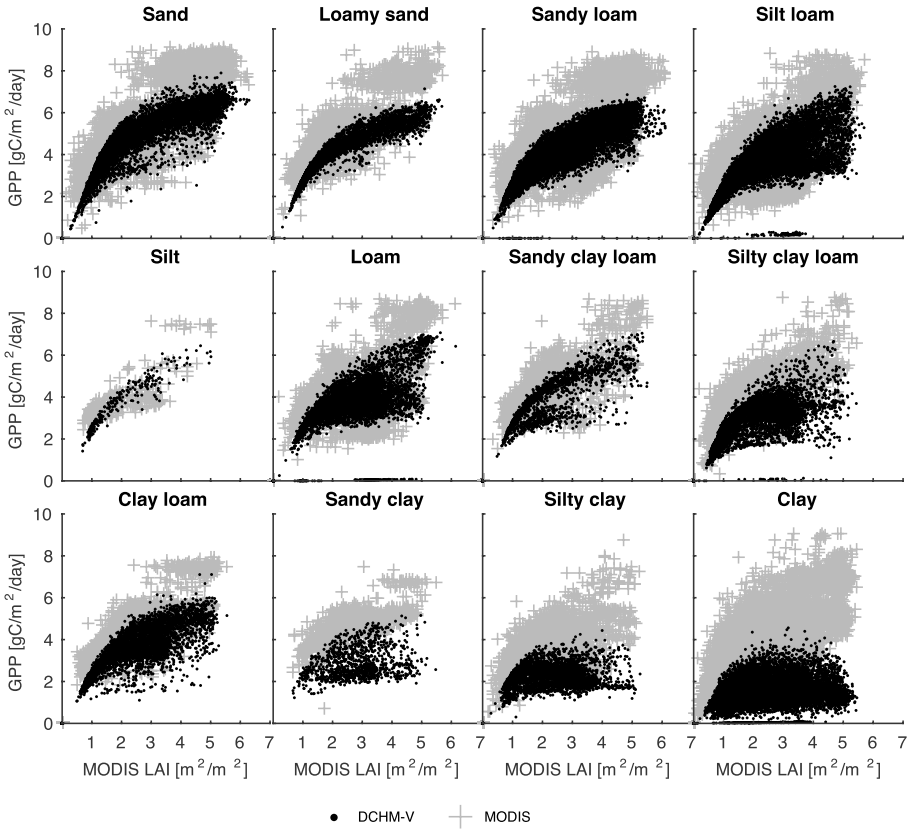

Figure 13. Relationship between average LAI and GPP in the DCHM-V and MODIS separated by soil texture in 2005. Note the nonlinear relationship in the DCHM-V data as a result of Beer's law scaling and the linear relationship in the MODIS data.

(August and September) and in quick succession (Table 2 and Figure 16). Before the first TC enters the domain, precipitation accumulations for the year are below the climatological average [*Brun and Barros*, 2014]. All of the TCs in this year influence rainfall patterns in the Appalachian Mountains and Piedmont regions (Figure 3). In Figure 16a, we demonstrate the immediate response to landfalling TCs

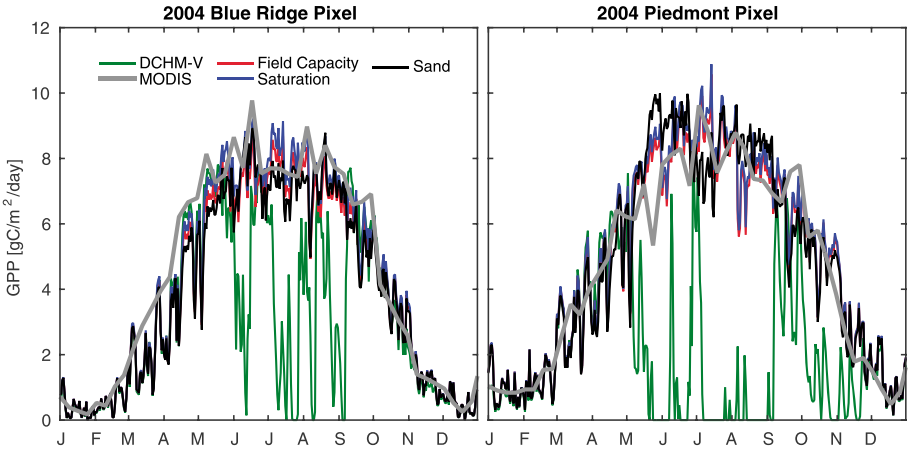

Figure 14. The 2004 GPP estimates from the DCHM-V With simulations (green), MODIS (gray), idealized soil moisture tests where soil moisture in the DCHM-V is fixed at field capacity (red) and saturation (blue), and soil texture experiment where soil type and hydraulic properties are consistent with sand (black).

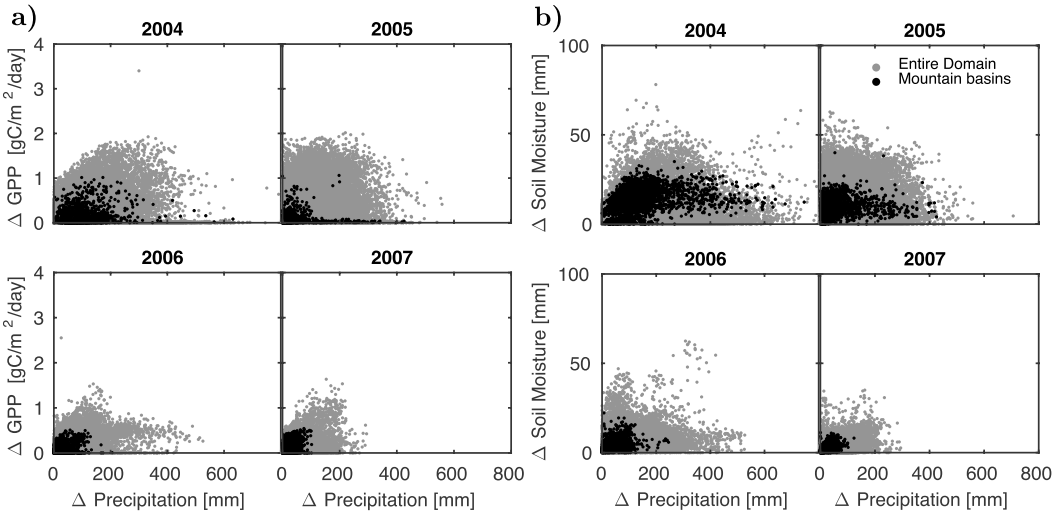

Figure 15. Scatterplots of the difference between DCHM-V With and Without simulations (Δ = With − Without): (a) precipitation input versus GPP output and (b) precipitation input versus soil moisture output. The black dots indicate domain grid cells located in intermountain basins (see Figure 1b).

during the 2004 hurricane season at each of the SE U.S. AmeriFlux towers. The towers are labeled by the distinct physiographic region in which they reside. As expected, the Piedmont locations show the strongest response with a positive increase in GPP when TCs are present in the forcing data. The Valley and Ridge locations have a smaller positive increase in GPP beginning after Hurricane Gaston, the third landfalling TC in 2004. Hurricane Gaston is the first TC of the season to have an eye track that does not follow exclusively along the coast, and the successive TCs of the season all follow inland tracks. The AmeriFlux towers in the Coastal Plain and Appalachian Plateaus do not see large changes in daily GPP, because these areas were farther from the TC eye tracks.

The TC trajectories in 2005 mostly followed paths to the west of the Appalachian Mountains, except for the final two storms of the season. Overall, the magnitude of the change in GPP associated with the presence of TCs is lower at the tower locations compared to 2004 and the arrival of TCs is spread out temporally over the course of the hurricane season (Figure 16b). The first three landfalling TCs in the domain are associated with higher GPP estimates in the Piedmont locations. Tropical Storm Arlene and Hurricanes Cindy and Dennis all have small impacts on precipitation across large portions of the domain including in the Inner Mountain and Piedmont regions [*Brun and Barros*, 2014]. Hurricanes Katrina and Rita only influence the western portion of the study domain, which is apparent in the simulations by a small increase in daily GPP for the locations in the Gulf Coastal Plains after Hurricane Katrina and very small increases after Hurricane Rita. Rainfall associated with the cloud shield from Tropical Storm Tammy generated a small increase in GPP in the Piedmont as the storm arrived late in the year. Hurricane Wilma did not impact the larger SE U.S. domain where the AmeriFlux towers are located.

In 2006, Tropical Storm Alberto arrived early in June and Hurricane Ernesto arrived late in the season in late August/early September. Tropical Storm Alberto's eye traveled through northern Florida and the Carolinas, and its impact on GPP is evident in the Florida Coastal Plain and the Piedmont regions (Figure 16c). While Alberto was a small storm, it has a net positive impact on GPP through the rest of the summer months due to otherwise dry conditions in these areas (Figure 16c). Hurricane Ernesto passed through the Carolinas and impacts GPP positively in the Piedmont and Valley and Ridge areas, although this impact diminishes after about a month as the growing season winds down.

The 2007 TC tracks influence few of the physiographic regions with storms bookending the growing season. The first storm of the year, Tropical Storm Barry, crosses through Florida during the end of May (peak growing season) and has a large impact on GPP for the Florida Coastal Plains locations and virtually no impact elsewhere in the SE U.S. (Figure 16d). The second storm, Tropical Storm Gabrielle made landfall in the Outer Banks of North Carolina in early September, never crosses into the main land and has negligible impacts on GPP in the domain. Hurricane Humberto's track is limited to the Gulf Coast and has a small impact on GPP estimates in the Gulf Coast and Valley and Ridge locations due to its arrival late in the growing season.

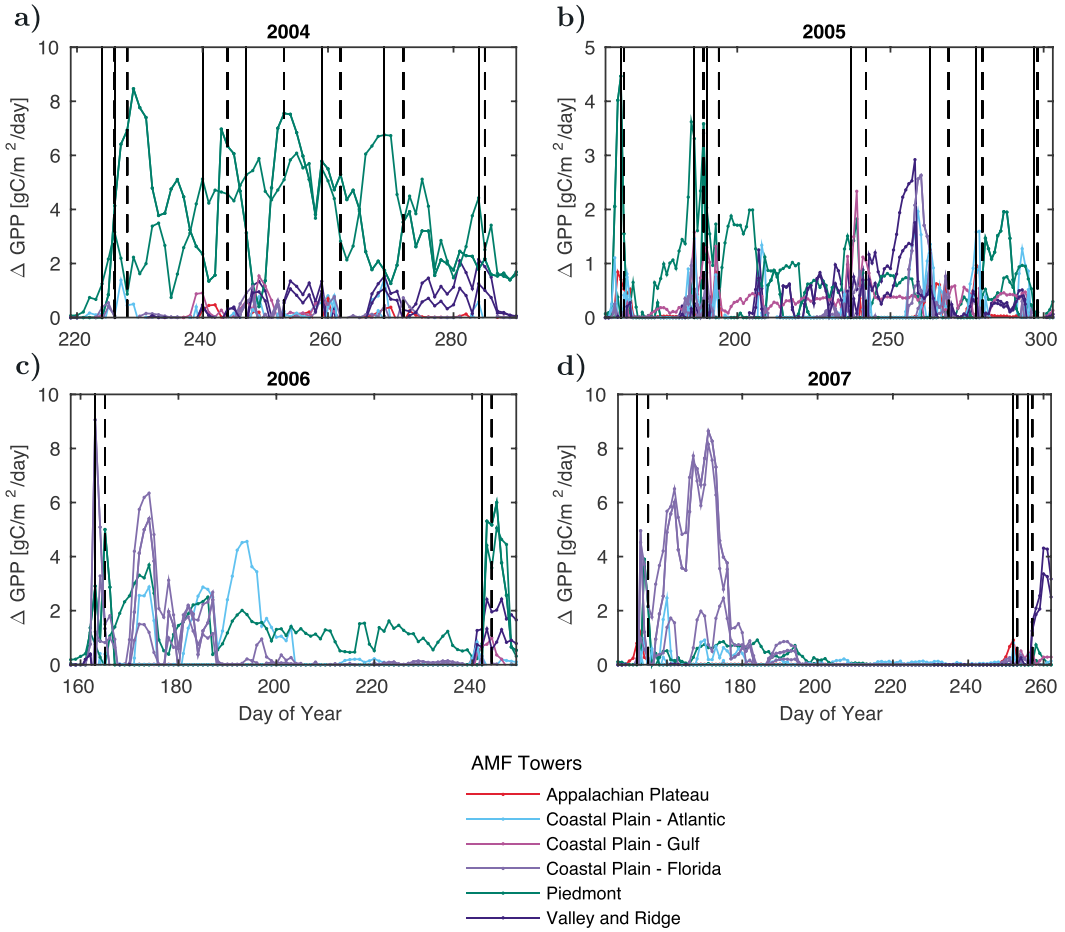

Figure 16. Difference in daily DCHM-V GPP (Δ = With − Without) at AmeriFlux tower locations labeled by physiographic regions (displayed in Figure 1a) for wet years and dry years: (a) 2004, (b) 2005, (c) 2006, and (d) 2007. TC landfall dates are marked by solid vertical black lines. TC exit dates are marked by dashed vertical black lines. Notice the difference in scales for the axes.

In summary, the impact of individual storms on vegetation activity depends on their trajectory and timing and antecedent soil moisture conditions. The 2004 storms have the largest impact because their eye tracks cross over the water-stressed Piedmont at the end of summer. In contrast, in 2005 there were a number of precipitation events not related to landfalling TCs and few storms impacted the water sensitive areas east of the Appalachians, resulting in smaller increases in GPP compared to 2004. In 2006, one large storm that made landfall in the Carolinas was able to impact the dry Piedmont soils in the midst of severe drought conditions, significantly increasing plant productivity locally. Small storms with short terrestrial trajectories provided little precipitation input and resulted in small increases in GPP in the region in 2007. The timing and tracks of TCs in the SE U.S. impact carbon assimilation rates with high interannual and intra-annual variability. Understanding this variability is key as forests in the SE U.S. are an important area for carbon sequestration [*McKinley et al.*, 2011; *Ryan et al.*, 2010; *Anderson et al.*, 2010]. Specifically, the SE U.S. contains the majority of temperate forests which act as a strong carbon sink due to their young age [*McKinley et al.*, 2011]. The Coastal Plains and Piedmont benefit the most from hurricane activity in the wet years with approximately three fourths of total change in GPP occurring in these regions (Table 4). In all, TCs positivity impact vegetation activity in 40–50% of the SE U.S. domain during wet years and increase regional GPP by 3–5 Mg C/m^2.

4.6. Study Limitations

The DCHM-V is not capturing effects of the mechanical destruction of vegetation by TCs directly in the With simulations; although indirectly this should be captured by the MODIS LAI and FPAR data sets used as phenology indicators. On the other hand, in the absence of a phenology model, the indirect TC impact of

vegetation loss is artificially retained in the Without simulations, due to a reliance on remotely sensed LAI to force the DCHM-V, which skews the results toward lower GPP differences between With and Without. This is of particular concern in the Without simulations where we modify the atmospheric forcing data as pointed out earlier. Vegetation disturbance as a result of TC activity is more pronounced in coastal and wetland areas impacted by saltwater intrusion associated with the storm surge and less pronounced in inland regions where trees may be uprooted and, or decrowned [*Brun and Barros*, 2013]. Wind damage can impact large areas of canopies and significantly reduce GPP at annual timescales, but even for very intense storms these disturbances are limited to coastlines [*Barr et al.*, 2012; *O'Halloran et al.*, 2012]. The result is a slight underestimation of GPP in the Without simulations because LAI is not adjusted to nonhurricane conditions, especially along coastlines. For the inland regions, higher water stress conditions in the Without simulations would result in lower LAI values [*Brun and Barros*, 2013]. Note, however, that much of the signature of mechanical disturbance in MODIS vegetation indices is smoothed by upscaling to 4 km resolution as shown by the uncertainty analysis in *Brun and Barros* [2013], even if along coastal areas and low-lying floodplains damages persist in the MODIS data. The uncertainty associated with these areas, however, will be small as low-lying coastal zones are less than 2% of the domain and the magnitude of productivity is low throughout the year compared to forest and savanna land cover types that make up the majority of the SE U.S. (Figure 1).

A further limitation that may impact the high sensitivity to water stress is the lack of connectivity between pixels in the model simulations. While the scale of individual grid cells (4 km × 4 km) suggests that the impact of redistribution would be negligible, previous applications of the DCHM-V at the basin scale demonstrate the importance of the contribution of subsurface flows in the redistribution of soil water and suggest that for regional events like TCs this effect is even more pronounced in complex terrain [*Tao and Barros,* 2013, 2014a; *Tao et al.*, 2016]. Because of fast response, these impacts are less important beyond the storm-scale rainfall-runoff response time at the 4 km resolution of the model implementation in this study but should be considered in the future.

Another limitation of the model formulation employed in this manuscript is the prescribed shallow soil depth of 1 m across the entire SE U.S. This impacts rooting depths and limits root water uptake to the imposed value in the model. Root phenology and response to soil water stress is complex and currently not accounted for in the DCHM-V. Better representation of root behavior would improve the representation of plant sensitivity to water stress demonstrated by the DCHM-V [*Wullschleger et al.*, 2002].

The weather in the reduced atmospheric forcing is strongly linked to the path, timing, and strength of the TCs originally present in the data. The systematic replacement of the atmospheric forcing data by the climatology over the entire domain alters conditions away from the TC paths as well. For example, small rain amounts are introduced where there was no rain in the atmospheric forcing away from the TC eye track. The reduced forcing will consistently overestimate precipitation during drought periods [*Brun and Barros*, 2014]. This implies that GPP should be overestimated in the Without simulations, and therefore, the difference between the With and Without simulations are lower bounds on the impact of TC precipitation. On the regional scale, this sensitivity study provides robust relative estimates of GPP changes due to changes in hydrologic processes caused by to the presence of TCs.

Regarding the representativeness of the Without TC simulations, we substitute the forcing over the entire SE U.S. domain rather than only over areas impacted by the TCs. One reason for not isolating individual areas is the difference in TC size and variable impact that each TC has over the domain at different time steps. Thus, replacing the signature of the 40 landfalling TCs between 2002 and 2012 becomes a difficult task. We caution here to limit analysis of spatial changes in GPP due to the presence of TCs to the quantifications provided in sections 3.2.2 and 4.5 because of the potential for anomalous behavior caused by replacing the signature of TCs broadly over the entire domain.

A next step is to conduct simulations with ensemble precipitation forcing and spatially variable soil depth to move toward a careful quantification of uncertainty [e.g., *Nogueira and Barros*, 2015].

5. Conclusions

The role of TCs in regional SE U.S. GPP estimates based on timing, eye track, landscape heterogeneity (i.e., soils, land use, and terrain), and antecedent moisture conditions was characterized using a coupled land surface, hydrology model with a biochemical representation of photosynthesis. The model results show that

the manner in which TCs alter the water budget reveals strong spatial organization reflecting the soils and regolith heterogeneity of the SE U.S. physiographic regions. Furthermore, there is large variability of individual TCs on productivity during the hurricane season: weak storms producing low precipitation fail to counteract drought conditions at all scales, whereas an intense storm producing heavy rainfall is sufficient to remedy drought conditions at local scales. The findings indicate TCs play an important role in maintaining soil water conditions favorable to carbon assimilation and provide a quantitative basis to assess the impacts of future climate scenarios conditional on hydrometeorological regime and water availability controls (soil moisture, fog, and clouds). In otherwise dry years with high TC activity, the impact on daily average GPP reflects TC trajectory relative to areas with the highest sensitivity to water stress, intensity and timing of the first storm, and interarrival times of subsequent storms. The annual impact of TCs on the study domain amounts to 9% of the warm season carbon uptake in the SE U.S. corresponding to about 3–5 Mg C/m^2 based on 2004–2005 values, which is roughly 2–3 orders of magnitude higher than the yearly total vehicle carbon emissions in the U.S.

This study shows that beyond their association with natural hazards, TCs are an important mechanism of terrestrial freshwater recharge that is closely tied to regional carbon assimilation capacity in the SE U.S. On decadal and longer timescales, at the intersection of climate and land use and land cover changes, changes in hurricane frequency and intensity can therefore have a major impact on net carbon sequestration that cannot be ignored.

Acknowledgments

The DCHM-V code is available upon request and the authors welcome any collaborative projects. Results from model simulations can be obtained from the authors upon request and available for downloading at http://iphex.pratt.duke.edu. This manuscript was motivated in part by exploratory work initiated by Julien Brun a former graduate student in the Barros group. The research was funded in part by current NSF award 1313799, CNH-Ex: Balancing Water Needs and Water Uses for Humans and Nature, and past NOAA SARP-WATER grant NA08OAR4310701. The NLDAS Phase 2 data used in this study were acquired as part of the mission of NASA's Earth Science Division and archived and distributed by the Goddard Earth Sciences (GES) Data and Information Services Center (DISC). The MODIS Collection 5 data products were retrieved from the online Data Pool, courtesy of the NASA Land Processes Distributed Active Archive Center (LP DAAC) and USGS/Earth Resources Observation and Science (EROS) Center, Sioux Falls, South Dakota, https://lpdaac.usgs.gov/data_access/data_pool.

References

Álvarez-Taboada, F., D. Tammadge, M. Schlerf, and A. Skidmore (2015), Assessing MODIS GPP in non-forested biomes in water limited areas using EC tower data, *Remote Sens.*, *7*, 3274–3292, doi:10.3390/rs70303274.

Amoozegar, A., P. J. Schoeneberger, and M. J. Vepraskas (1991), Characterization of soils and saprolites from the Piedmont region for waste-disposal purposes, Rep. PB-92-183763/XAB; UNC-WRRI--91-255, North Carolina Water Resour. Res. Inst., Raleigh, NC.

Anderson, R. G., et al. (2010), Biophysical considerations in forestry for climate protection, *Front. Ecol. Environ.*, *9*, 174–182, doi:10.1890/090179.

Baldocchi, D. (1997), Flux footprints within and over forest canopies, *Boundary Layer Meteorol.*, *85*, 273–292, doi:10.1023/A:1000472717236.

Baldocchi, D. (2003), Assessing the eddy covariance technique for evaluating carbon dioxide exchange rates of ecosystems: Past, present and future, *Global Change Biol.*, *9*, 479–492, doi:10.1046/j.1365-2486.2003.00629.

Baldocchi, D., et al. (2001), FLUXNET: A new tool to study the temporal and spatial variability of ecosystem–scale carbon dioxide, water vapor, and energy flux densities, *Bull. Am. Meteorol. Soc.*, *82*, 2415–2434, doi:10.1175/1520-0477.

Baldwin, M. E., and K. E. Mitchell (1998), Progress on the NCEP hourly multi-sensor U.S. precipitation analysis for operations and GCIP research, Preprints, paper presented at 2nd Symposium on Integrated Observing Systems, Am. Meteorol. Soc., Phoenix, Ariz., 10-11.

Barlow, M. (2011), Influence of hurricane-related activity on North American extreme precipitation, *Geophys. Res. Lett.*, *38*, L04705, doi:10.1029/2010GL046258.

Barr, J. G., V. Engel, T. J. Smith, and J. D. Fuentes (2012), Hurricane disturbance and recovery of energy balance, CO2 fluxes and canopy structure in a mangrove forest of the Florida Everglades, *Agric. Forest Meteorol.*, *153*, 54–66, doi:10.1016/j.agrformet.2011.07.022.

Barros, A. P. (1995), Adaptive multilevel modeling of land-atmosphere interactions, *J. Clim.*, *8*, 2144–2160.

Berry, Z. C., and W. K. Smith (2013a), Ecophysiological importance of cloud immersion in a relic spruce–fir forest at elevational limits, southern Appalachian Mountains, USA, *Oecologia*, *173*, 637–648, doi:10.1007/s00442-013-2653-4.

Berry, Z. C., and W. K. Smith (2013b), Experimental cloud immersion and foliar water uptake in saplings of Abies fraseri and Picea rubens, *Trees Struct. Funct.*, *28*, 115–123, doi:10.1007/s00468-013-0934-5.

Brennan, M. J., R. D. Knabb, M. Mainelli, and T. B. Kimberlain (2009), Atlantic hurricane season of 2007, *Mon. Weather Rev.*, *137*, 4061–4088, doi:10.1175/2009MWR2995.1.

Brun, J., and A. P. Barros (2013), Vegetation activity monitoring as an indicator of eco-hydrological impacts of extreme events in the southeastern USA, *Int. J. Remote Sens.*, *34*, 519–544, doi:10.1080/01431161.2012.714088.

Brun, J., and A. P. Barros (2014), Mapping the role of tropical cyclones on the hydroclimate of the southeast United States: 2002–2011, *Int. J. Climatol.*, *34*, 494–517, doi:10.1002/joc.3703.

Buol, S. W., and S. B. Weed (1991), Saprolite-soil transformations in the Piedmont and Mountains of North Carolina, *Geoderma*, *51*, 15–28, doi:10.1016/0016-7061(91)90064-Z.

Chambers, J. Q., J. I. Fisher, H. Zeng, E. L. Chapman, D. B. Baker, and G. C. Hurtt (2007), Hurricane Katrina's carbon footprint on U.S. Gulf Coast Forests, *Science*, *318*, 1107–1107, doi:10.1126/science.1148913.

Chen, J., P. Jönsson, M. Tamura, Z. Gu, B. Matsushita, and L. Eklundh (2004), A simple method for reconstructing a high-quality NDVI time-series data set based on the Savitzky-Golay filter, *Remote Sens. Environ.*, *91*, 332–344, doi:10.1016/j.rse.2004.03.014.

Clark, K. L., H. L. Gholz, and M. S. Castro (2004), Carbon dynamics along a chronosequence of slash pine plantations in north Florida, *Ecol. Appl.*, *14*, 1154–1171, doi:10.1890/02-5391.

Cosgrove, B. A., et al. (2003), Real-time and retrospective forcing in the North American Land Data Assimilation System (NLDAS) project, *J. Geophys. Res.*, *108*(D22), 8842, doi:10.1029/2002JD003118.

Cry, G. W. (1967), *Effects of Tropical Cyclone Rainfall on the Distribution of Precipitation Over the Eastern and Southern United States*, U.S. Dept. of Commerce, Environ. Sci. Serv. Admin., Washington.

Desai, A. R., et al. (2008), Cross-site evaluation of eddy covariance GPP and RE decomposition techniques, *Agric. Forest Meteorol.*, *148*, 821–838, doi:10.1016/j.agrformet.2007.11.012.

Devonec, E., and A. P. Barros (2002), Exploring the transferability of a land-surface hydrology model, *J. Hydrol.*, *265*, 258–282.

Duan, Y., A. M. Wilson, and A. P. Barros (2015), Scoping a field experiment: Error diagnostics of TRMM precipitation radar estimates in complex terrain as a basis for IPHEx2014, *Hydrol. Earth Syst. Sci.*, *19*, 1501–1520, doi:10.5194/hess-19-1501-2015.

Dwyer, J., and G. Schmidt (2006), The MODIS reprojection tool, in *Earth Science Satellite Remote Sensing*, edited by J. J. Qu et al., pp. 162–177, Springer, Berlin.

Eimers, J. L., S. Terziotti, and M. J. Giorgino (2001), Estimated depth to water, North Carolina, USGS. [Available at http://nc.water.usgs.gov/reports/ofr01487/index.html.]

Eller, C. B., A. L. Lima, and R. S. Oliveira (2013), Foliar uptake of fog water and transport belowground alleviates drought effects in the cloud forest tree species, Drimys brasiliensis (Winteraceae), *New Phytol.*, *199*, 151–162, doi:10.1111/nph.12248.

Elsner, J. B., J. P. Kossin, and T. H. Jagger (2008), The increasing intensity of the strongest tropical cyclones, *Nature*, *455*, 92–95, doi:10.1038/nature07234.

Emanuel, K. A. (1987), The dependence of hurricane intensity on climate, *Nature*, *326*, 483–485, doi:10.1038/326483a0.

Falge, E., et al. (2002), Seasonality of ecosystem respiration and gross primary production as derived from FLUXNET measurements, *Agric. Forest Meteorol.*, *113*, 53–74.

Farquhar, G. D., and S. von Caemmerer (1982), Modelling of photosynthetic rate to environmental conditions, in *Physiological plant ecology II: Water relations and carbon assimilation*, vol. 12, edited by B. O. L. Lange et al., pp. 549–587, Springer, Berlin.

Farquhar, G. D., S. von Caemmerer, and J. A. Berry (1980), A biochemical model of photosynthetic CO2 assimilation in leaves of C3 species, *Planta*, *149*, 78–90, doi:10.1007/BF00386231.

Franklin, J. L., and D. P. Brown (2008), Atlantic hurricane season of 2006, *Mon. Weather Rev.*, *136*, 1174–1200, doi:10.1175/2007MWR2377.1.

Friend, A. D. (1995), PGEN: An integrated model of leaf photosynthesis, transpiration, and conductance, *Ecol. Model.*, *77*, 233–255, doi:10.1016/0304-3800.

Galarneau, T. J., L. F. Bosart, and R. S. Schumacher (2010), Predecessor rain events ahead of tropical cyclones, *Mon. Weather Rev.*, *138*, 3272–3297, doi:10.1175/2010MWR3243.1.

Garcia-Quijano, J. F., and A. P. Barros (2005), Incorporating canopy physiology into a hydrological model: Photosynthesis, dynamic respiration, and stomatal sensitivity, *Ecol. Model.*, *185*, 29–49, doi:10.1016/j.ecolmodel.2004.08.024.

Gebremichael, M., and A. P. Barros (2006), Evaluation of MODIS gross primary productivity (GPP) in tropical monsoon regions, *Remote Sens. Environ.*, *100*, 150–166, doi:10.1016/j.rse.2005.10.009.

Gilmanov, T. G., et al. (2010), Productivity, respiration, and light-response parameters of world grassland and agroecosystems derived from flux-tower measurements, *Rangeland Ecol. Manag.*, *63*, 16–39, doi:10.2111/REM-D-09-00072.1.

Goulden, M. L., J. W. Munger, S.-M. Fan, B. C. Daube, and S. C. Wofsy (1996), Measurements of carbon sequestration by long-term eddy covariance: Methods and a critical evaluation of accuracy, *Global Change Biol.*, *2*, 169–182, doi:10.1111/j.1365-2486.1996.tb00070.x.

Grant, R. F., A. G. Barr, T. A. Black, H. A. Margolis, J. H. McCaughey, and J. A. Trofymow (2010), Net ecosystem productivity of temperate and boreal forests after clearcutting—A Fluxnet-Canada measurement and modelling synthesis, *Tellus B*, *62*, 475–496, doi:10.1111/j.1600-0889.2010.00500.x.

Hamilton, J. G., E. H. DeLucia, K. George, S. L. Naidu, A. C. Finzi, and W. H. Schlesinger (2002), Forest carbon balance under elevated CO2, *Oecologia*, *131*, 250–260, doi:10.1007/s00442-002-0884-x.

Hargrove, W. W., F. M. Hoffman, and B. E. Law (2003), New analysis reveals representativeness of the AmeriFlux network, *Eos Trans. AGU*, *84*, 529–535, doi:10.1029/2003EO480001.

Hart, R. E., and J. L. Evans (2001), A Climatology of the extratropical transition of Atlantic tropical cyclones, *J. Clim.*, *14*, 546–564, doi:10.1175/1520-0442(2001)014.

Heinsch, F. A., et al. (2003), User's Guide: GPP and NPP (MOD17A2/A3) Products, NASA MODIS Land Algorithm, Version 2.0, Univ. of Montana, Missoula, 57 pp.

Heinsch, F. A., et al. (2006), Evaluation of remote sensing based terrestrial productivity from MODIS using regional tower eddy flux network observations, *IEEE T. Geosci. Remote Sens.*, *44*, 1908–1925.

Held, I. M., and M. Zhao (2011), The response of tropical cyclone statistics to an increase in CO2 with fixed sea surface temperatures, *J. Clim.*, *24*, 5353–5364, doi:10.1175/JCLI-D-11-00050.1.

Henderson-Sellers, A., et al. (1998), Tropical cyclones and global climate change: A post-IPCC assessment, *Bull. Am. Meteorol. Soc.*, *79*, 19–38, doi:10.1175/1520-0477(1998)079.

Hutley, L. B., B. J. Evans, J. Beringer, G. D. Cook, S. W. Maier, and E. Razon (2013), Impacts of an extreme cyclone event on landscape-scale savanna fire, productivity and greenhouse gas emissions, *Environ. Res. Lett.*, *8*, 045023, doi:10.1088/1748-9326/8/4/045023.

Johnson, D. M., and W. K. Smith (2006), Low clouds and cloud immersion enhance photosynthesis in understory species of a southern Appalachian spruce–fir forest (USA), *Am. J. Bot.*, *93*, 1625–1632, doi:10.3732/ajb.93.11.1625.

Jönsson, P., and L. Eklundh (2004), TIMESAT—A program for analyzing time-series of satellite sensor data, *Comput. Geosci.*, *30*, 833–845, doi:10.1016/j.cageo.2004.05.006.

Kam, J., J. Sheffield, X. Yuan, and E. F. Wood (2012), The influence of Atlantic tropical cyclones on drought over the eastern United States (1980–2007), *J. Clim.*, *26*, 3067–3086, doi:10.1175/JCLI-D-12-00244.1.

Kashian, D. M., W. H. Romme, D. B. Tinker, M. G. Turner, and M. G. Ryan (2006), Carbon storage on landscapes with stand-replacing fires, *BioScience*, *56*, 598–606, doi:10.1641/0006-3568(2006)56.

Kim, H.-S., G. A. Vecchi, T. R. Knutson, W. G. Anderson, T. L. Delworth, A. Rosati, F. Zeng, and M. Zhao (2014), Tropical cyclone simulation and response to CO2 doubling in the GFDL CM2.5 high-resolution coupled climate model, *J. Clim.*, *27*, 8034–8054, doi:10.1175/JCLI-D-13-00475.1.

Knight, D. B., and R. E. Davis (2007), Climatology of tropical cyclone rainfall in the southeastern United States, *Phys. Geogr.*, *28*, 126–147, doi:10.2747/0272-3646.28.2.126.

Knutson, T. R., and R. E. Tuleya (2004), Impact of CO_2-induced warming on simulated hurricane intensity and precipitation: Sensitivity to the choice of climate model and convective parameterization, *J. Clim.*, *17*, 3477–3495, doi:10.1175/1520-0442(2004)017.

Konrad, C. E., and L. B. Perry (2010), Relationships between tropical cyclones and heavy rainfall in the Carolina region of the USA, *Int. J. Climatol.*, *30*, 522–534.

Kossin, J. P., K. A. Emanuel, and G. A. Vecchi (2014), The poleward migration of the location of tropical cyclone maximum intensity, *Nature*, *509*, 349–352, doi:10.1038/nature13278.

Koster, R., and M. Suarez (1994), The components of a SVAT scheme and their effects on a GCM's hydrological cycle, *Adv. Water Resour.*, *17*, 61–78.

Koster, R., and M. Suarez (1996), Energy and water balance calculations in the Mosaic LSM, NASA Tech. Memo., 104606, 9, 60 pp.

Lai, C.-T., G. Katul, J. Butnor, D. Ellsworth, and R. Oren (2002), Modelling night-time ecosystem respiration by a constrained source optimization method, *Global Change Biol.*, *8*, 124–141, doi:10.1046/j.1354-1013.2001.00447.x.

Lighthill, J., G. Holland, W. M. Gray, C. Landsea, G. Craig, J. Evans, Y. Kurihara, and C. P. Guard (1994), Global climate change and tropical cyclones, *Bull. Am. Meteorol. Soc.*, *75*, 2147–2157.

Lin, Y., and K. E. Mitchell (2005), The NCEP Stage II/IV hourly precipitation analyses: Development and applications, paper presented at 19th Conference on Hydrology, Am. Meteorol. Soc., San Diego, Calif., Pap. 1.2.

Land Processes Distributed Active Archive Center (2006), Land Processes Distributed Active Archive Center, dataset: NASA EOSDIS Land Processes DAAC, USGS Earth Resources Observation and Science (EROS) Center, Sioux Falls, South Dakota. [Available at https://lpdaac.usgs.gov, accessed January 1, 2015.]

Luo, Y., B. Medlyn, D. Hui, D. Ellsworth, J. Reynolds, and G. Katul (2001), Gross primary productivity in duke forest: Modeling synthesis of CO_2 experiment and eddy–flux data, *Ecol. Appl.*, *11*, 239–252, doi:10.1890/1051-0761(2001)011.

Ma, S., D. D. Baldocchi, L. Xu, and T. Hehn (2007), Inter-annual variability in carbon dioxide exchange of an oak/grass savanna and open grassland in California, *Agr. Forest Meteorol.*, *147*, 157–171, doi:10.1016/j.agrformet.2007.07.008.

Macdonald, J. R. (1972), Are the data worth owning?, *Science*, *176*, 1377.

Manzoni, S., G. Vico, G. Katul, P. A. Fay, W. Polley, S. Palmroth, and A. Porporato (2011), Optimizing stomatal conductance for maximum carbon gain under water stress: A meta-analysis across plant functional types and climates, *Funct. Ecol.*, *25*, 456–467, doi:10.1111/j.1365-2435.2010.01822.x.

Markewich, H. W., M. J. Pavich, and G. R. Buell (1990), Contrasting soils and landscapes of the Piedmont and Coastal Plain, eastern United States, *Geomorphology*, *3*, 417–447, doi:10.1016/0169-555X(90)90015-I.

Maxwell, J. T., P. T. Soulé, J. T. Ortegren, and P. A. Knapp (2012), Drought-busting tropical cyclones in the southeastern Atlantic United States: 1950–2008, *Ann. Assoc. Am. Geogr.*, *102*, 259–275, doi:10.1080/00045608.2011.596377.

McGrath, G. S., R. Sadler, K. Fleming, P. Tregoning, C. Hinz, and E. J. Veneklaas (2012), Tropical cyclones and the ecohydrology of Australia's recent continental-scale drought, *Geophys. Res. Lett.*, *39*, L03404. doi:10.1029/2011GL050263

McKinley, D. C., et al. (2011), A synthesis of current knowledge on forests and carbon storage in the United States, *Ecol. Appl.*, *21*, 1902–1924, doi:10.1890/10-0697.1.

McNulty, S. G. (2002), Hurricane impacts on US forest carbon sequestration, *Environ. Pollut.*, *116*(Suppl. 1), S17–S24, doi:10.1016/S0269-7491(01)00242-1.

Meehl, G. A., and C. Tebaldi (2004), More intense, more frequent, and longer lasting heat waves in the 21st century, *Science*, *305*, 994–997, doi:10.1126/science.1098704.

Melillo, J. M., T. C. Richmond, and G. W. Yohe (Eds.) (2014), *Climate change impacts in the United States: The Third National Climate Assessment*, 841 pp., U.S. Global Change Research Program, doi:10.7930/J0Z31WJ2.

Michalakes, J., S. Chen, J. Dudhia, L. Hart, J. Klemp, J. Middlecoff, and W. Skamarock (2001), Development of a next generation regional weather research and forecast model, in *Developments in Teracomputing: Proceedings of the Ninth ECMWF Workshop on the Use of High Performance Computing in Meteorology*, edited by W. Zwieflhofer and N. Kreitz, pp. 269–276 , World Scientific, Singapore.

Miller, D. A., and R. A. White (1998), A conterminous United States multilayer soil characteristics dataset for regional climate and hydrology modeling, *Earth Interact.*, *2*, 1–26, doi:10.1175/1087-3562.

Mitchell, K. E., et al. (2004), The multi-institution North American Land Data Assimilation System (NLDAS): Utilizing multiple GCIP products and partners in a continental distributed hydrological modeling system, *J. Geophys. Res.*, *109*, D07S90, doi:10.1029/2003JD003823.

Monteith, J. L. (1972), Solar radiation and productivity in tropical ecosystems, *J. Appl. Ecol.*, *9*, 747–766, doi:10.2307/2401901.

Nogueira, M., and A. P. Barros (2015), Transient stochastic downscaling of quantitative precipitation estimates for hydrological applications, *J. Hydrol.*, *529*(Part 3), 1407–1421, doi:10.1016/j.jhydrol.2015.08.041.

Nogueira, R. C., and B. D. Keim (2010), Contributions of Atlantic tropical cyclones to monthly and seasonal rainfall in the eastern United States 1960–2007, *Theor. Appl. Climatol.*, *103*, 213–227, doi:10.1007/s00704-010-0292-9.

Noormets, A., M. J. Gavazzi, S. G. McNulty, J.-C. Domec, G. Sun, J. S. King, and J. Chen (2010), Response of carbon fluxes to drought in a coastal plain loblolly pine forest, *Global Change Biol.*, *16*, 272–287, doi:10.1111/j.1365-2486.2009.01928.x.

O'Halloran, T. L., et al. (2012), Radiative forcing of natural forest disturbances, *Global Change Biol.*, *18*, 555–565, doi:10.1111/j.1365-2486.2011.02577.x.

Oren, R., B. E. Ewers, P. Todd, N. Phillips, and G. Katul (1998), Water balance delineates the soil layer in which moisture affects canopy conductance, *Ecol. Appl.*, *8*, 990–1002, doi:10.1890/1051-0761.

Oren, R., C.-I. Hsieh, P. Stoy, J. Albertson, H. R. McCarthy, P. Harrell, and G. G. Katul (2006), Estimating the uncertainty in annual net ecosystem carbon exchange: Spatial variation in turbulent fluxes and sampling errors in eddy-covariance measurements, *Global Change Biol.*, *12*, 883–896, doi:10.1111/j.1365-2486.2006.01131.x.

Pataki, D. E., and R. Oren (2003), Species differences in stomatal control of water loss at the canopy scale in a mature bottomland deciduous forest, *Adv. Water Resour.*, *26*, 1267–1278, doi:10.1016/j.advwatres.2003.08.001.

Prat, O. P., and A. P. Barros (2010a), Ground observations to characterize the spatial gradients and vertical structure of orographic precipitation—Experiments in the inner region of the Great Smoky Mountains, *J. Hydrol.*, *391*, 141–156, doi:10.1016/j.jhydrol.2010.07.013.

Prat, O. P., and A. P. Barros (2010b), Assessing satellite-based precipitation estimates in the Southern Appalachian mountains using rain gauges and TRMM PR, *Adv. Geosci.*, *25*, 143–153, doi:10.5194/adgeo-25-143-2010.

Rawls, W. J., and D. L. Brakensiek (1982), Estimating soil water retention from soil properties, *J. Irrig. Drain. Div. ASCE*, *108*, 166–171.

Rawls, W. J., T. J. Gish, and D. L. Brakensiek (1991), Estimating soil water retention from soil physical properties and characteristics, *Adv. Soil Sci.*, *16*, 213–234.

Rawls, W. J., L. R. Ahuja, D. L. Brakensiek, and A. Shirmohammadi (1993), Infiltration and soil water movement, in *Handbook of hydrology*, edited by D. R. Maidment, McGraw-Hill, New York.

Richardson, A. D., D. Y. Hollinger, D. B. Dail, J. T. Lee, J. W. Munger, and J. O'keefe (2009), Influence of spring phenology on seasonal and annual carbon balance in two contrasting New England forests, *Tree Physiol.*, *29*, 321–331, doi:10.1093/treephys/tpn040.

Running, S. W., P. E. Thornton, R. R. Nemani, and J. M. Glassy (2000), Global terrestrial gross and net primary productivity from the Earth observing system, in *Methods in Ecosystem Science*, edited by O. Sala et al., pp. 44–57 , Springer-Verlag, New York.

Running, S. W., R. R. Nemani, F. A. Heinsch, M. Zhao, M. Reeves, and H. Hashimoto (2004), A continuous satellite-derived measure of global terrestrial primary production, *BioScience*, *54*, 547–560, doi:10.1641/0006-3568.

Ryan, M. G., et al. (2010), A synthesis of the science on forests and carbon for U.S. Forests, *Issues Ecol.*, *13*, 1–16.

Schäfer, K. V. R., R. Oren, D. S. Ellsworth, C.-T. Lai, J. D. Herrick, A. C. Finzi, D. D. Richter, and G. G. Katul (2003), Exposure to an enriched CO_2 atmosphere alters carbon assimilation and allocation in a pine forest ecosystem, *Global Change Biol.*, *9*, 1378–1400, doi:10.1046/j.1365-2486.2003.00662.x.

Sheffield, J., and E. F. Wood (2007), Projected changes in drought occurrence under future global warming from multi-model, multi-scenario, IPCC AR4 simulations, *Clim. Dyn.*, *31*, 79–105, doi:10.1007/s00382-007-0340-z.

Stoy, P. C., G. G. Katul, M. B. S. Siqueira, J.-Y. Juang, K. A. Novick, J. M. Uebelherr, and R. Oren (2006), An evaluation of models for partitioning eddy covariance-measured net ecosystem exchange into photosynthesis and respiration, *Agric. For. Meteorol.*, *141*, 2–18, doi:10.1016/j.agrformet.2006.09.001.

Sun, G., et al. (2011), Upscaling key ecosystem functions across the conterminous United States by a water-centric ecosystem model, *J. Geophys. Res.*, *116*, G00J05, doi:10.1029/2010JG001573.

Tao, J., and A. P. Barros (2013), Prospects for flash flood forecasting in mountainous regions—An investigation of Tropical Storm Fay in the Southern Appalachians, *J. Hydrol.*, *506*, 69–89, doi:10.1016/j.jhydrol.2013.02.052.

Tao, J., and A. P. Barros (2014a), Coupled prediction of flood response and debris flow initiation during warm- and cold-season events in the Southern Appalachians, USA, *Hydrol. Earth Syst. Sci.*, *18*, 367–388, doi:10.5194/hess-18-367-2014.

Tao, J., and A. P. Barros (2014b), The Integrated Precipitation and Hydrology Experiment. Part I: Quality High-Resolution Landscape Attributes Datasets, Rep. EPL-2013-IPHEX-H4SE-1, Duke University, Durham, NC, V.1., 60 pp., doi:10.7924/G8H41PBG.

Tao, J., D. Wu, J. Gourley, S. Q. Zhang, W. Crow, C. Peters-Lidard, and A. P. Barros (2016), Operational hydrological forecasting during the IPHEx-IOP campaign—Meet the challenge, *J. Hydrol.*, doi:10.1016/j.jhydrol.2016.02.019.

Thornley, J. H. M., and M. G. R. Cannell (2000), Modelling the components of plant respiration: Representation and realism, *Ann. Bot.*, *85*, 55–67, doi:10.1006/anbo.1999.0997.

Tian, H., G. Chen, M. Liu, C. Zhang, G. Sun, C. Lu, X. Xu, W. Ren, S. Pan, and A. Chappelka (2010), Model estimates of net primary productivity, evapotranspiration, and water use efficiency in the terrestrial ecosystems of the southern United States during 1895–2007, *Forest Ecol. Manag.*, *259*, 1311–1327, doi:10.1016/j.foreco.2009.10.009.

Turner, D. P., S. Urbanski, D. Bremer, S. C. Wofsy, T. Meyers, S. T. Gower, and M. Gregory (2003), A cross-biome comparison of daily light use efficiency for gross primary production, *Global Change Biol.*, *9*, 383–395, doi:10.1046/j.1365-2486.2003.00573.x.

Uriarte, M., and M. Papaik (2007), Hurricane impacts on dynamics, structure and carbon sequestration potential of forest ecosystems in Southern New England, USA, *Tellus A*, *59*, 519–528, doi:10.1111/j.1600-0870.2007.00243.x.

Verma, M., et al. (2014), Remote sensing of annual terrestrial gross primary productivity from MODIS: An assessment using the FLUXNET La Thuile data set, *Biogeosciences*, *11*, 2185–2200, doi:10.5194/bg-11-2185-2014.

Vicente-Serrano, S. M., et al. (2013), Response of vegetation to drought time-scales across global land biomes, *Proc. Natl. Acad. Sci. U.S.A.*, *110*, 52–57, doi:10.1073/pnas.1207068110.

Villarini, G., J. A. Smith, M. L. Baeck, T. Marchok, and G. A. Vecchi (2011), Characterization of rainfall distribution and flooding associated with U.S. landfalling tropical cyclones: Analyses of Hurricanes Frances, Ivan, and Jeanne (2004), *J. Geophys. Res.*, *116*, D23116, doi:10.1029/2011JD016175.

Wilson, A. M., and A. P. Barros (2014), An investigation of warm rainfall microphysics in the Southern Appalachians: Orographic enhancement via low-level seeder-feeder interactions, *J. Atmos. Sci.*, *5*(5), 1783–1805.

Wilson, A. M., and A. P. Barros (2015), Landform controls on low level moisture convergence and the diurnal cycle of warm season orographic rainfall in the Southern Appalachians, *J. Hydrol.*, *531*, 475–493.

Wooten, R. M., K. A. Gillon, A. C. Witt, R. S. Latham, T. J. Douglas, J. B. Bauer, S. J. Fuemmeler, and L. G. Lee (2007), Geologic, geomorphic, and meteorological aspects of debris flows triggered by Hurricanes Frances and Ivan during September 2004 in the Southern Appalachian Mountains of Macon County, North Carolina (southeastern USA), *Landslides*, *5*, 31–44, doi:10.1007/s10346-007-0109-9.

Wullschleger, S. D., T. J. Tschaplinski, and R. J. Norby (2002), Plant water relations at elevated CO_2—Implications for water-limited environments, *Plant Cell Environ.*, *25*, 319–331, doi:10.1046/j.1365-3040.2002.00796.x.

Xia, Y., et al. (2012), Continental-scale water and energy flux analysis and validation for the North American Land Data Assimilation System project phase 2 (NLDAS-2): 1. Intercomparison and application of model products, *J. Geophys. Res.*, *117*, D03109, doi:10.1029/2011JD016048.

Yildiz, O. (2001), Assessment and simulation of hydrologic extremes by a physically-based spatially distributed hydrologic model, PhD Dissertation, Department of Civil and Environmental Engineering, The Pennsylvania State University, University Park, Pa., 214 pp.

Yildiz, O., and A. P. Barros (2005), Climate variability, water resources, and hydrologic extremes—Modeling the water and energy budgets, in *Climate and Hydrology, in Mountain Areas*, edited by C. de Jong, et al., John Wiley, Chichester, U. K., doi:10.1002/0470858249.ch20.

Yildiz, O., and A. P. Barros (2007), Elucidating vegetation controls on the hydroclimatology of a mid-latitude basin, *J. Hydrol.*, *333*, 431–448, doi:10.1016/j.jhydrol.2006.09.010.

Yildiz, O., and A. P. Barros (2009), Evaluating spatial variability and scale effects on hydrologic processes in a midsize river basin, *Sci. Res. Essays*, *4*, 217–225.

Yuan, H., Y. Dai, Z. Xiao, D. Ji, and W. Shangguan (2011), Reprocessing the MODIS leaf area index products for land surface and climate modelling, *Remote Sens. Environ.*, *115*, 1171–1187, doi:10.1016/j.rse.2011.01.001.

Zeng, H., J. Q. Chambers, R. I. Negrón-Juárez, G. C. Hurtt, D. B. Baker, and M. D. Powell (2009), Impacts of tropical cyclones on U.S. forest tree mortality and carbon flux from 1851 to 2000, *Proc. Natl. Acad. Sci. U.S.A.*, *106*, 7888–7892, doi:10.1073/pnas.0808914106.

Zhang, Y., C. Song, G. Sun, L. E. Band, A. Noormets, and Q. Zhang (2015), Understanding moisture stress on light use efficiency across terrestrial ecosystems based on global flux and remote-sensing data, *J. Geophys. Res. Biogeosci.*, *120*, 2053–2066, doi:10.1002/2015JG003023.

Zhao, M., and S. W. Running (2010), Drought-induced reduction in global terrestrial net primary production from 2000 through 2009, *Science*, *329*, 940–943, doi:10.1126/science.1192666.

Erratum

In the originally published version of this article, in Tables 2 and 4 and other instances where the units Mg C/m^2 appear in the text, these values correspond to a sum of fluxes for all pixels rather than an average flux. These are different interpretations and to reduce confusion with regards to the units the values should be multiplied by the domain grid cell area (16 sq. km) to obtain a cumulative mass. This information is provided for clarification; the originally published article files are correct, and may be considered the authoritative version of record.